Title: **The fat body cortical actin network regulates *Drosophila* inter-organ nutrient trafficking and adipocyte cell size**

Authors: Rupali Ugrankar[1], Son Tran[1], Jade Bowerman[1,2], Anastasiia Kovalenko[1,3], Blessy Paul[1], W. Mike Henne[1,*]

Affiliations:
[1]Department of Cell Biology, UT Southwestern Medical Center, Dallas, TX 75390, USA
[2]present address: Department of Molecular Biology and Genetics, Cornell University, Ithaca, NY 14850, USA
[3]present address: ETH Zürich, Institute of Biochemistry, Department of Biology, Otto-Stern-Weg 3, 8093 Zürich, Switzerland.

*please address correspondence to: mike.henne@utsouthwestern.edu

Abstract:

Defective nutrient storage and adipocyte enlargement (hypertrophy) are emerging features of metabolic syndrome and type 2 diabetes. How the cytoskeletal network contributes to nutrient uptake, fat storage, and adipocyte size remain poorly understood. Utilizing the *Drosophila* larval fat body (FB) as a model adipose tissue, we show that a specific actin isoform—Act5C—forms the cortical actin network necessary for inter-organ lipid trafficking. Act5C also promotes FB tissue expansion during larval development so larvae can store sufficient biomass for metamorphosis. We find FB-specific loss of Act5C, but not other *Drosophila* actins, perturbs FB triglyceride (TG) storage in lipid droplets (LDs), resulting in developmentally delayed larvae that fail to develop into flies. Act5C localizes to the FB cell surface where it intimately contacts peripheral LDs (pLDs), forming a cortical actin network together with spectrins for cell architectural support. While both the cortical actin and spectrin cytoskeletons maintain FB cell surface architecture, we find that only the actin network is required for fat storage. Mechanistically, we show that FBs lacking the Act5C cortical cytoskeleton exhibit a block in lipoprotein (Lpp) secretion from FB cells, and a subsequent disruption of gut:FB inter-organ lipid transport, resulting in mid-gut fat accumulation. Utilizing temporal RNAi-depletion approaches, we also reveal that Act5C is indispensable post-embryogenesis during larval feeding to promote FB cell expansion. Act5C-deficient FBs fail to expand cell sizes, leading to lipodystrophic larvae unable to accrue sufficient biomass for metamorphosis. Collectively, we propose that the Act5C-mediated cortical actin network of *Drosophila* adipose tissue plays an essential role in post-embryonic inter-organ nutrient transport and FB cell size determination for organismal energy homeostasis and development.

Introduction:

Adipocytes are specialized nutrient storage cells that exhibit the remarkable ability to alter their size in response to metabolic challenges such as nutrient excess or development. In mammals, high-nutrient diets can drive the dramatic expansion of adipocyte cell size, termed hypertrophy, that enables them to absorb and store elevated nutrients as fat, thus avoiding lipotoxicity and ensuring metabolic homeostasis (Hansson et al., 2019; Virtue and Vidal-Puig, 2010). Dysfunctional hypertrophy is a recognized feature of diseases such as obesity and type 2 diabetes, but the mechanisms governing adipocyte cell size determination and expansion remain poorly understood (Nunn et al., 2022). In *Drosophila*, the central metabolic organ regulating energy storage and signaling is the fat body (FB), functionally analogous to the mammalian adipose tissue and liver (Arrese and Soulages, 2010; Musselman et al., 2013; Musselman and Kühnlein, 2018). Adipogenesis is completed during late embryogenesis when FB cells merge into a single-cell thick continuous tissue comprising of ~2200 cells primed to store nutrients including triglycerides (TG) in lipid droplets (LDs) and glycogen for energy homeostasis (Bharucha, 2009; Hoshizaki et al., 1994; Yongmei Xi, 2015)**.** Upon hatching, young larvae immediately begin feeding and growing; dietary carbohydrates, proteins, and fats are absorbed and metabolized by the gut. Lipids, in the form of diacylglycerol (DAG), are delivered to other organs including the FB though inter-organ transport (Heier et al., 2021; Palm et al., 2012)**.** During larval development FB cells do not increase in number, but instead expand enormously in size over a 4-5 day period to accommodate the TG stores and biomass necessary for metamorphosis (Meschi and Delanoue, 2021; Yongmei Xi, 2015). Thus, through three instar stages (L1-L3), feeding larvae increase ~200x in overall biomass, much of which consists of FB LDs (Pirahas et al., 2021; Jacobs, 2020).

Defects in FB nutrient storage can result in larvae failing to reach their 'critical weight' (CW), defined as the minimum threshold weight at which 50% of larvae can proceed to pupation without further feeding (De Moed et al., 1999; Juarez-Carreño et al., 2021; Nijhout and Williams, 1974; Tennessen and Thummel, 2011). This can occur (in part) due to a block in inter-organ lipid trafficking and uptake. Such trafficking is primarily mediated by lipoproteins (Lpp) in the blood-like hemolymph. Circulating Lpp particles receive DAG lipids from the gut, then traverse the hemolymph to deliver them to the FB for LD storage. Lpp particles are themselves synthesized and secreted by FB cells, and loss of FB Lpp production or secretion perturbs inter-organ nutrient flux, causing lipid accumulation in the mid-gut and developmental arrest prior to

pupation (Heier et al., 2021; Matsuo et al., 2019; Palm et al., 2012). Thus, advancement past the CW checkpoint and successful metamorphosis requires coordination in nutrient uptake, transport, storage, and expenditure during *Drosophila* development (Merkey et al., 2011; Nijhout and Williams, 1974; Schönborn et al., 2019; Tennessen and Thummel, 2011). Although studied for over 40 years, a pervasive question in *Drosophila* development is what cellular factors influence larval CW attainment, and how inter-organ communication governs nutrient storage in the FB for CW.

To execute its diverse functions, the FB requires architectural organization. One such architectural feature is the cytoskeleton, composed of protein polymers including F-actin and spectrins that form supportive scaffolds within the FB (Brozinick et al., 2007; Köster and Mayor, 2016). In fact, the cytoskeletons of both *Drosophila* and mammalian adipose tissues play essential roles in cell homeostasis and nutrient storage, and this relies on poorly characterized mechanisms involving actin dynamics. For example, the actin network of mammalian pre-adipocytes undergoes dramatic remodeling during adipocyte differentiation (Hansson et al., 2019; Liu et al., 2006). Whereas pre-adipocytes exhibit intracellular actin stress fibers, mature adipocytes accumulate F-actin at the cell surface, forming a cortical actin network together with the spectrin protein fodrin that supports the caveolae-rich surface membrane (Kanzaki and Pessin, 2002; Kim et al., 2019). Mice fed a high fat diet also exhibit a significant expansion of adipocyte cell size (i.e., hypertrophy) that requires cytoskeletal rearrangements to harbor fat stores (Hansson et al., 2019). How this rearrangement is coordinated remains enigmatic, but enlarged adipocytes exhibit increased F-actin pools and elevated actin modulating factors, suggesting increased lipid accumulation correlates with actin polymerization. In mice, adipocyte actin networks can regulate the delivery of glucose transporters like Glut4 to cell surfaces for carbohydrate uptake, but whether this is a general regulatory feature of actin networks in adipose tissues remains unclear (Brozinick et al., 2007; Kanzaki and Pessin, 2002; Kim et al., 2019). Thus, a key knowledge gap is understanding how the cortical cytoskeleton of adipose tissues contributes to extracellular nutrient uptake, fat storage, inter-organ lipid trafficking, and adipose tissue expansion, all of which the *Drosophila* FB must coordinate to enable successful development of larvae into flies.

Drosophila actins share 98% similarity with humans (Schroeder et al., 2021). While humans have as many as 20 actins, *Drosophila* express six: 2 cytoplasmic isoforms (Act5C and Act42A), 2 larval muscle isoforms (Act57B and Act87E), and 2 adult muscle actins (Act79B and Act88F)

(Burn et al., 1989; Röper et al., 2005; Wagner et al., 2002). Despite their close relation, actin isoforms are not functionally redundant, as substituting one for another does not always rescue the phenotype arising from the missing isoform. This may be because these actins exhibit highly regulated expression patterns both in tissues and across organismal development (Wagner et al., 2002). Within the FB, F-actin contributes to tissue support and cohesion, but its roles in nutrient and metabolic homeostasis are underexplored.

Here, we utilize the *Drosophila* larval FB as a model adipose tissue to dissect the role of the cortical cytoskeleton in nutrient storage and animal development. We find that the *Drosophila* actin isoform Act5C forms the larval FB cortical actin network, and is uniquely required for FB lipid and tissue homeostasis. FB-specific loss of Act5C, but not other actin isoforms, perturbs larval TG storage, producing small lipodystrophic larvae exhibiting eventual developmental arrest. We also find that loss of the actin and spectrin networks differentially impact FB nutrient storage, suggesting these two cortical cytoskeletal systems uniquely influence FB homeostasis. Mechanistically, disruption of the FB cortical actin network does not perturb carbohydrate nor lipid uptake itself, but surprisingly reduces Lpp secretion from the FB, thus perturbing gut:FB inter-organ lipid trafficking. Finally, we utilize a temporal genetic manipulation approach to reveal that Act5C is not required for embryogenesis, but for post-embryonic larval growth and biomass accumulation. Specifically, we find Act5C is necessary for FB cell size expansion and biomass accrual during larval feeding and growth. Thus, loss of post-embryonic Act5C leads to small FB cells, lipodystrophy, and developmental arrest. Collectively, we identify a non-canonical role for the cortical actin network of *Drosophila* FB cells in regulating Lpp-mediated inter-organ trafficking, and propose that cortical actin networks influence adipocyte cell size and tissue growth critical for organismal development.

Results:

Act5C forms a cortical actin network in the larval fat body

To determine how the actin network is organized within the *Drosophila* larval fat body (FB), we extracted FBs from w^{1118} (laboratory control strain) non-wandering L3 larvae, fixed and labeled these with the fluorescent F-actin stain phalloidin, and conducted confocal z-section microscopy. We found that most F-actin was highly polarized to FB cell surfaces exposed to the hemolymph, as well as intra-tissue cell-cell boundaries, with a dim intracellular pool also detectable (**Figure 1A**). Imaging revealed that the cortical F-actin localized to microridge protrusions at the tissue surface, giving the FB surface a “foamy” appearance consistent with

previous reports showing the plasma membrane of FB cells is densely ruffled (Diaconeasa et al., 2013; Ugrankar et al., 2019) **(Figure 1A**).

FB cells contain abundant triglyceride (TG) stores in cytoplasmic lipid droplets (LDs). A sub-population of small LDs are localized to the cell periphery next to the tissue surface (defined as peripheral LDs, pLDs), whereas larger LDs are packed in the cell interior close to the tissue mid-plane (defined as medial LDs, mLDs) (Ugrankar et al., 2019). We examined how this F-actin framework was spatially arranged in relation to pLDs and mLDs. Z-section confocal microscopy of FBs stained with the fluorescent F-actin dye Cell Mask™ Actin Tracking Stain, together with LD dye monodansylpentane (MDH), revealed a bright ruffled cortical F-actin cytoskeleton intimately arranged around small pLDs, appearing to encircle many pLDs adjacent to the cell surface (**Figure 1B**, **red arrows**). Side-profile *yx-axis* views revealed the actin:pLD arrangement was particularly evident at hemolymph-exposed FB cell surfaces. In contrast, in the tissue interior the actin network did not encircle individual mLDs.

Since the functional relationship between the actin cytoskeleton and LDs in adipose tissues is not well understood, we began to dissect their interplay using *Drosophila* FBs. First, we utilized a candidate-based visual screen to identify the specific actin isoforms required for the FB cortical actin network. *Drosophila* express six actin isoforms (Act5C, Act42A, Act57B, Act79D, Act87E, and Act88F) in various tissues (Burn et al., 1989; Röper et al., 2005; Wagner et al., 2002). We RNAi depleted each actin isoform specifically in the FB using the FB tissue-specific driver *Dcg-Gal4,* and stained for F-actin. Strikingly, FB-specific RNAi depletion of Act5C (*Dcg-Gal4>UAS-Act5C*^{RNAi}), but not any other actin isoforms, dramatically altered F-Actin polarization to cell surfaces and cell-cell boundaries, leaving only intracellular actin pools (**Figure 1C, Figure Supplement 1A**). Line-scans confirmed that the major F-actin surface enrichment was ablated in *Act5C*^{RNAi} FB tissue, indicating the Act5C isoform was necessary for the FB cortical actin network (**Figure Supplement 1A**). Additionally, the FB cell surface now appeared smooth and lacked its microridge patterning, suggesting Act5C, but not other actin isoforms, was required for this “foamy” surface appearance (**Figure 1C, red boxes are single FB cells**).

To confirm Act5C can form a cortical actin network, we directly imaged Act5C in the FB by expressing *UAS-Act5C-GFP* using the *Dcg-Gal4* driver. Similar to the phalloidin and Cell Mask™ Actin staining, Act5C-GFP decorated FB cell surfaces and enriched at cell-cell interfaces (**Figure 1D**). Act5C-GFP also intimately wrapped around pLDs at the cell periphery

(**Figure 1D, red arrows**). To understand how this cortical actin network relates to the cell surface, we co-expressed *UAS-Act5C-RFP* together with the plasma membrane (PM) marker *UAS-mCD8-GFP.* This revealed that the Act5C cortical actin network and PM are closely overlaid, and both exhibit the microridge pattern intimately encircling pLDs (**Figure 1E, red arrows, Figure Supplement 1B**). Collectively, we conclude that Act5C is required for forming the FB cortical actin network, and that it is in close proximity to the cell PM, as well as pLDs adjacent to the cell surface.

FB-specific Act5C loss drastically alters LD morphology and TG storage

Given that Act5C localizes in close proximity to LDs at the cell surface, we next examined how FB-specific Act5C depletion impacted LDs and fat storage. To quantitatively access this, we measured size changes of mLDs and pLDs in larval FBs in which each actin isoform was depleted. Notably loss of Act5C, but not other actin isoforms, significantly altered both mLD and pLD morphologies (**Figure 2A,B, Figure Supplement 2A,B**). Specifically, Act5C loss significantly increased the average size of pLDs, and drastically reduced the average size of mLDs **(Figure 2A-D**). In contrast, RNAi depletion of all the other actin isoforms did not drastically alter the average sizes of either LD pool, although there was a mild increase in average mLD size in *Act57B*^{RNAi} tissues (**Figure 2D, Figure Supplement 2A**).

To determine whether Act5C loss also impacted larval triglyceride (TG) storage, we measured TG abundance in *Act5C*^{RNAi} and control whole larvae. Consistent with their altered LD morphologies, FB-specific Act5C depletion significantly reduced larval TG levels, which were ~10% of 6-day age-matched controls (**Figure 2E**). Since TG levels are influenced by both lipogenesis as well as TG lipolysis, we employed qPCR to evaluate the expression levels of known lipogenesis and lipolysis factors in isolated FB tissues. Whereas major *de novo* lipogenesis genes like acetyl-CoA carboxylase (ACC) and the fatty acid synthase (FASN) were expressed at normal levels in *Act5C*^{RNAi} FB compared to controls, genes for TG production including GPAT4, the diacylglycerol acyltransferase (DGAT) enzyme MDY, and the fatty acid desaturase DESAT1 were significantly reduced in expression, suggesting a defect in TG synthesis (**Figure 2F**). To determine whether this TG reduction was caused in part by increased lipid mobilization, we also examined expression levels of lipolysis-associated genes. However, the expression of the TG lipolysis enzyme Brummer (BMM), as well as mitochondrial fatty acid oxidation importer CPT1, were significantly reduced, suggesting the observed TG reduction was not a result of elevated lipolysis nor enhanced fatty acid oxidation (**Figure 2F**). Collectively, this

suggests that Act5C loss in the FB drastically alters LD morphologies and reduces TG pools, likely due to reduced TG synthesis.

FB-specific Act5C loss leads to small, developmentally delayed larvae that fail to develop into flies

Drosophila Act5C global mutants die as first instar larvae due to arrested growth (Wagner et al., 2002), but we noted that FB-specific Act5C depletion produced viable larvae that could proceed through larval development and sometimes pupate. However, we found that age-matched L3 Act5C FB-deficient larvae were undersized compared to pre-wandering controls, suggesting a developmental arrest or significant delay (**Figure 2G**). Consistent with this, control larvae began wandering and pupating between days ~5 to 6 after egg laying (AEL), whereas there was a significant delay in wandering of Act5C-deficient larvae (**Figure 2I**). *Act5C*^{RNAi} larvae lingered in the food for an additional 7 to 14 days, gradually increasing their overall size to nearly match controls. However, these developmentally delayed larvae appeared transparent, and upon imaging were lipodystrophic with small FBs compared to controls (**Figure 2K**). TG levels of these 21-day larvae were higher than at day 6, but still much less than L3 pre-wandering control larvae (**Figure 2E**). Some of these larger larvae did wander and pupate, but became necrotic during metamorphosis and failed to eclose to adult flies (**Figure 2H, J, red arrows denote necrotic pupae**). Indeed, FBs extracted from wandering *Act5C*^{RNAi} larvae showed underdeveloped lobes with significantly smaller FB cells, suggesting that Act5C was required for normal FB development and cell size (**Figure 2L,M,N**). Collectively, this indicates that the Act5C-dependent cortical actin network is required for proper TG storage in the FB, as well as contributes to proper FB tissue growth, larval growth, and FB cell size.

Loss of the cortical actin and spectrin cytoskeletons differentially alter FB lipid homeostasis

Since the FB cortical cytoskeleton is composed of both F-actin and spectrin networks (Brozinick et al., 2007; Köster and Mayor, 2016), we next investigated how each contributed to FB tissue homeostasis and fat storage. To interrogate the spectrin network, we examined the roles of alpha-spectrin and beta-spectrin, which hetero-dimerize to provide architectural support to the tissue at the cell surface (Brozinick et al., 2007; Köster and Mayor, 2016). We also examined Twinfilin (Twf), a F-actin effector protein that binds monomeric actin and promotes F-actin turnover (Moseley et al., 2006). Loss of Twf reduces F-actin turnover and stabilizes F-actin filaments (**Figure 3A**).

First, we examined how loss of alpha/beta-spectrin compared to Act5C loss with respect to FB LD homeostasis. We RNAi depleted each spectrin in the FB and examined LDs by confocal microscopy. Similar to Act5C loss, depletion of either beta-spectrin or alpha-spectrin caused a significant increase in average pLD size (**Figure 3B,C, Figure Supplement 3A**). However, alpha- or beta-spectrin loss did not alter the mLD population, suggesting perturbation of the spectrin network impacted only LDs near the cell surface, but not LDs globally (**Figure 3D**). This was distinct from Act5C loss, which drastically altered both pLDs and mLDs (**Figure 3B,C,D**). When we examined how larval TG levels were impacted by spectrin loss, we noted that loss of alpha-spectrin did not significantly alter TG levels from controls, and beta-spectrin depletion surprisingly elevated larval TG levels, the opposite effect of Act5C loss (**Figure 3E**). Altogether, this indicates that ablation of the cortical actin and spectrin networks have different effects on FB LDs and TG storage.

To dissect if perturbing F-actin dynamics would impact LDs and TG stores, we next examined LDs in *Twf*^{RNAi} FBs. We found Twf loss did reduce pLD density at the cell surface, but did not alter pLD size (**Figure 3B,C, Figure Supplement 3A**). Like Act5C loss, Twf depletion also significantly reduced mLD sizes (**Figure 3B,D**). In line with this, larval TG levels were significantly decreased in *Twf*^{RNAi} larvae, albeit to a milder degree than Act5C loss (**Figure 3E**). To confirm that Twf loss was actually impacting F-actin turnover, we phalloidin-stained control and *Twf*^{RNAi} FBs. Indeed, Twf-depleted tissues manifested more intense cortical F-actin stain, and FB cell surfaces now exhibited bright phalloidin-positive puncta, consistent with decreased actin turnover (**Figure 3F**). Collectively, this suggests that either loss of Act5C or perturbation of F-actin turnover perturbs both pLDs and mLDs, as well as reduces total larval TG stores.

Next, we examined how loss of Act5C and the spectrin network impacted the FB cell surface architecture and its microridge network. Whereas control FB tissues displayed “foamy” microridges that surrounded pLDs when labeled with the cell surface marker mCD8-RFP, loss of either Act5C or beta-spectrin ablated this surface ruffling (**Figure 3G, red arrows**). Tissue surfaces now appeared smooth and small pLDs were absent, with only large LDs adjacent to the surface. This suggested that the microridge architecture required contributions from both F-actin and spectrins to properly form, and that these microridges influence the small sizes of pLDs. Collectively, we find that the cortical actin and spectrin networks differentially regulate FB LD homeostasis and TG storage. Loss of either Act5C or the spectrins impacts cell surface

architecture and its contacts with pLDs. As such, loss of Act5C or spectrins alters pLD sizes. However, whereas spectrins primarily influence only pLD sizes, loss of Act5C or Twf impacts both pLD and mLDs sizes, as well as overall TG levels. Thus, the cortical actin and spectrin cytoskeletal systems appear to have distinct roles in FB tissue lipid homeostasis, but a shared role in maintaining FB cell surface architecture.

Cortical actin network loss does not reduce FB lipid or carbohydrate uptake

Given that loss of Act5C or perturbation of F-Actin turnover (Twf) impacted FB LDs and TG stores, we next focused on mechanistically dissecting how the actin cytoskeleton contributes to fat storage. A recent model using mice adipocytes suggests that the F-actin network regulates TG storage by influencing the trafficking of carbohydrate transporters like Glut4 to the cell surface, and thus regulating carbohydrate uptake into adipocytes for eventual storage as TG (Brozinick et al., 2007; Kim et al., 2019). To determine whether the FB cortical actin network influenced nutrient uptake, we developed fluorescence-based nutrient uptake assays. First, we determined whether Act5C loss affected FB carbohydrate absorption. We extracted FB tissues from pre-starved (to deplete glycogen stores (Yamada et al., 2018)), control or Act5C FB-deficient larvae, and exposed them to PBS media containing 2-NBD-glucose (2-NBDG) (**Figure 4A**). 2-NBDG was dimly detected in the cytoplasm of FB cells, and appeared at least as abundant in Act5C-depleted FB tissues as in controls, suggesting Act5C loss did not reduce the ability of FB tissue to absorb extracellular carbohydrates (**Figure 4B,C**).

Next, we examined whether Act5C loss impacted FB lipid absorption. We exposed extracted larval FB tissues to PBS media containing BODIPY-C12, a fluorescently-conjugated fatty acid that can be internalized by cells and incorporated into TG (Kasurinen, 1992). Intracellular BODIPY-C12 could be detected in both control and Act5C depleted FB tissues (**Figure 4 D,E,F**). Surprisingly, the BODIPY-C12 signal in FBs from *Act5C*^{RNAi} larvae was significantly higher compared to controls, suggesting Act5C loss did not inhibit the capability of FBs to absorb extracellular lipids, and in fact Act5C loss may actually promote extracellular lipid absorption (**Figure 4E,F**).

Carbohydrate uptake and its conversion to TG help *Drosophila* larvae maintain circulating blood/hemolymph sugar levels (Havula et al., 2013; Sassu et al., 2012). Therefore, we also examined whether Act5C loss altered hemolymph carbohydrate levels *in vivo*. We monitored circulating hemolymph levels of both glucose and trehalose in control and FB-specific *Act5C*^{RNAi}

larvae, and found neither was altered (**Figure 4G,H**). Like the *ex vivo* experiments, this suggested carbohydrate uptake into the FB was not perturbed with Act5C loss, and rather may be more efficient considering larvae have reduced total fat tissue mass, which is the major carbohydrate sink (Musselman et al., 2013). Similarly, levels of FB glycogen, the storage form of carbohydrates, were not significantly different between control and FB-specific Act5C^{RNAi} larvae (**Figure 4I,J**). Lastly, to test if FB tissues could deliver carbohydrate transporters to the cell surface for uptake from circulation, we imaged a GFP-tagged model glucose transporter, hGlut4-GFP (Crivat et al., 2013) expressed in larval FBs, and found it could be successfully delivered to the surface of Act5C-deficient FB cells (**Figure 4K**). Collectively this indicates that Act5C loss does not interfere with the capability of the FB to absorb extracellular nutrients, and thus cannot be majorly responsible for the reduced TG levels observed in Act5C-deficient FBs.

FB-specific Act5C depletion perturbs lipoprotein-mediated inter-organ lipid trafficking

Since Act5C-depleted FBs appeared capable of absorbing extracellular nutrients, we next examined whether there was a defect in delivering nutrients to the FB. The primary mechanism for FB lipid delivery is through lipoprotein (Lpp)-mediated inter-organ trafficking in the hemolymph, between the animal gut to the FB. Lpp particles (also called lipophorins) are initially manufactured within FB cells, then secreted into the hemolymph to facilitate inter-organ lipid transport (Heier and Kühnlein, 2018; Matsuo et al., 2019; Palm et al., 2012) (**Figure 5A**). Defects in Lpp-mediated lipid trafficking lead to lipid accumulation in the mid-gut, which can be visualized as LDs (Palm et al., 2012). Since Act5C-deficient FBs displayed reduced TG storage but were capable of nutrient uptake, we next interrogated whether there was a defect in this gut:FB inter-organ lipid transport.

First, we isolated non-wandering L3 larval guts and stained for LDs using Nile Red. Strikingly, whereas control mid-guts exhibited small sparse LDs, mid-guts from larvae with FB-specific Act5C-depletion displayed significant fat accumulation, and closely resembled larvae lacking Lpp (*ApoLpp*^{RNAi}), implying a defect in mid-gut lipid export (**Figure 5B**). Additionally, FB-specific *Twf*^{RNAi} also resulted in significant fat accumulation in larval mid-guts, indicating that perturbation of F-actin turnover in the FB also resulted in a similar gut fat accumulation (**Figure 5B**). To quantify relative gut fat accumulation, we isolated guts from these larvae and measured TG levels. Indeed, both Act5C and Twf FB-depletion significantly elevated gut TG compared to controls (**Figure 5C**). As expected, loss of ApoLpp also increased gut TG levels (**Figure Supplement 5A**). In contrast, beta-spectrin loss in the FB actually *decreased* gut TG levels

versus control tissue, and only a few, sparse LDs were observed in these mid-guts, underscoring the different functional consequences to larval physiology when the FB actin versus spectrin networks are perturbed (**Figure 5B,C**).

To more directly evaluate how FB actin loss impacted circulating lipids and inter-organ lipid trafficking, we next measured larval hemolymph lipids. Consistent with defective inter-organ trafficking, Act5C loss in the FB significantly reduced hemolymph DAG, the major Lpp-associated lipid (**Figure 5D**). Hemolymph DAG pools also trended downward in Twf FB-deficient conditions, but were just below significance threshold. In contrast, *beta-spectrin*^{RNAi} hemolymph DAG was unaltered compared to controls, again indicating that in contrast to loss of the actin network, loss of the FB spectrin network did not impact circulating lipid pools (**Figure 5D**). Since hemolymph isolation from ApoLpp-depleted larvae proved challenging, we instead measured whole-larval DAG pools, which were significantly decreased from controls, consistent with the established role of Lpp in trafficking DAG between larval tissues (**Figure Supplement 5B**).

Act5C loss in the FB alters the spatial distribution of Lpp-like particles

Since hemolymph DAG is bound to Lpp particles that are synthesized and secreted by the FB (Heier and Kühnlein, 2018; Palm et al., 2012), we hypothesized that Act5C loss impacted Lpp production and/or secretion from FB cells. To interrogate this, we immuno-stained for Lpp particles in control and Act5C-deficient extracted larval FB tissues. Notably, in control tissues Lpp particles were concentrated in the FB cell periphery (**Figure 5E**). In fact, high resolution imaging indicated that Lpp particles formed bright clusters in close proximity to pLDs adjacent to the cell surface (**Figure 5E, red arrows**). This was intriguing, and appeared similar to the known spatial distribution of lipoprotein particles in human hepatocytes, which express the Lpp homolog Apoprotein B (ApoB) that is assembled and lipidated with TG in ER sub-domains immediately adjacent to LDs (Taghibiglou et al., 2000; Ye et al., 2009). Furthermore, our previous work indicated that depletion of *Drosophila* Lpp particles in larvae impacted pLD homeostasis, suggesting a functional connection between pLDs and Lpp particles at the FB surface (Ugrankar et al., 2019).

To further probe the similarities between *Drosophila* Lpp particles and human ApoB, we cultured human Huh7 hepatocytes and immuno-stained for ApoB in cells also co-stained for the ER network and LDs. This confirmed that ApoB forms puncta and crescent-like structures in ER

sub-domains adjacent to LDs that appeared very similar to the Lpp-like IF puncta we observed in larval FB cells (**Figure Supplement 5C**). Next, we imaged anti:Lpp-stained larval FBs depleted of Act5C. *Act5C*^{RNAi} FBs, like controls, also displayed a bright Lpp immuno-stain, indicating that Lpp production itself was not affected by loss of Act5C. However, Lpp localization and distribution drastically differed in *Act5C*^{RNAi} versus control tissues. In striking contrast to controls, Act5C-deficient FBs lost Lpp polarization to the cell periphery, and instead exhibited diffuse Lpp signal throughout the FB cell interior (**Figure 5E**). This Lpp immuno-signal also localized to a reticulated network that appeared similar to the ER, implying Act5C loss caused some defect in Lpp intra-cellular organization and/or secretion.

To gain higher resolution insights into the spatial organization of Lpp particles within *Drosophila* FB cells, we conducted thin-section transmission electron microscopy (TEM) on intact larval FBs. In control tissues, we observed grape-like particle clusters in close proximity of LDs that appeared very similar to the Lpp fluorescence immuno-staining (**Figure 5F red arrows, Figure Supplement 5D red arrows**). These particles were ~60nm in diameter, in close agreement to the expected sizes of Lpp particles (Wojczynski et al., 2011). In further support of this, previous work showing TEM of locust FBs revealed similarly sized Lpp particles (Dantuma et al., 1998). Furthermore, we observed some particles in the microridge folds at the FB cell surface, indicating they may be secreted by FB cells (**Figure Supplement 5D, blue stars**). In Lpp-depleted FB TEM sections (*Dcg-Gal4>ApoLpp*^{RNAi}) these particles were not present, supporting that they were Lpp particles (**Figure 5F, Figure Supplement 5D**). Interestingly, TEM of *Act5C*^{RNAi} FB tissues revealed that the Lpp-like particles did not accumulate near LDs, and they now distributed diffuse throughout the cell interior, similar to the anti-Lpp immuno-signal, and further supporting the model that these particles were indeed intracellular Lpp, and that loss of Act5C perturbed their secretion (**Figure 5E, F, Figure Supplement 5D**).

Collectively, this suggests that the Act5C-dependent cortical actin network is required for normal Lpp particle organization and secretion from FB cells into the larval hemolymph. Defects from Act5C loss in FBs result in lower hemolymph DAG pools, as well as fat accumulation in the gut.

Loss of canonical secretory proteins mimics Act5C depletion in the FB

As our observations supported a model where Act5C was required for FB Lpp secretion, perturbation of this process may explain (at least in part) the reduced LD and TG storage defects observed in Act5C-depleted FB tissues. To further interrogate this, we compared Act5C

depletion to loss of known secretory pathway factors in the FB. We RNAi depleted the known secretory protein Sar1, an Arf family GTPase that promotes ER-to-Golgi trafficking, as well as Tango1, an ER-to-Golgi trafficking factor (Yang et al., 2021). Indeed, FB-specific loss of either Sar1 or Tango1 caused similar defects as Act5C loss. This included similar accumulation of LDs and TG increases in the larval gut (**Figure 5B,C**). Sar1 and Tango1 loss also mirrored Act5C FB depletion in that they exhibited decreased whole-larvae TG levels (**Figure Supplement 5E**), significantly decreased hemolymph DAG pools (**Figure 5D**), and larvae developed L3 developmental arrest, consistent with a block in Lpp secretion and inter-organ lipid transport. This supports a model where loss of either Act5C or known secretion-associated machinery reduces hemolymph Lpp levels and subsequent gut:FB lipid trafficking. As an additional interrogation of how Act5C loss impacted the FB cell secretory pathway, we imaged *UAS-dGRASP65-GFP*, a known Golgi marker protein. As expected, dGRASP65-GFP marked numerous Golgi foci in control FB tissues, particularly in the cell periphery just below the surface (**Figure Supplement 5F**). However, dGRASP65-GFP foci were reduced in abundance in Act5C-depleted FBs, particularly in the mid-plane, indicating Act5C loss impacted Golgi homeostasis in the FB.

Collectively, this suggests that Act5C and the cortical actin network are required for normal Lpp particle secretion into the larval hemolymph, and the subsequent lipid release from the gut and inter-organ lipid transport required for normal TG storage in the FB. In line with this, both Lpp and Act5C depletion in the FB appear to cause reductions in larval size, and both lead to developmental arrest. It should also be noted that Act5C loss does not appear to cause a general block in all FB membrane trafficking, as the PM marker mCD8-GFP as well as the PM-localized glucose transporter hGlut4-GFP both localize to the surfaces of larval FB cells following FB-specific Act5C-depletion (**Figure 3G, Figure 4K**).

Act5C is required in the FB for post-embryonic larval development

Given that a FB pool of Act5C is necessary for normal larval inter-organ lipid trafficking, we next interrogated when Act5C was required in the larval developmental timeline. To enable temporal control over Act5C expression during development we employed the Gal4/Gal80 system (McGuire et al., 2004). Gal80 is a temperature sensitive allele that at lower temperatures (18°C) prevents Gal4 from binding to the UAS (Upstream Activating Sequences), thereby repressing activation of the Act5C TRiP RNAi transgene. Upon switching to 29°C, Gal80 is degraded, allowing Gal4 to bind UAS sequences and drive FB-specific (Dcg-Gal4 mediated) knockdown of

Act5C. First, we allowed *Dcg-Gal4; tub-Gal80ts X UAS-Act5C*^{RNAi} parents to lay eggs at 29°C, which were maintained at this non-permissive (Act5C is RNAi-depleted, Act5C^{OFF}) temperature through embryogenesis (i.e. 1 day). We then lowered the culturing temperature to the permissive 18°C for the remainder of larval development to enable Act5C expression (Act5C^{ON}). Surprisingly, this 1-day Act5C depletion during embryogenesis still enabled larvae to successfully develop into flies, suggesting Act5C is not functionally required in the FB during embryogenesis itself (**Figure 6A**). Importantly, this also implies that Act5C was not essential for initial adipogenesis or FB cell differentiation, as these are known to occur during late embryogenesis (Hoshizaki et al., 1994; Yongmei Xi, 2015).

Next, we extended the non-permissive 29°C treatment for 2-days and 3-days, depleting Act5C during embryogenesis and through the L1 and/or L2 stages of larval development. Indeed, vials cultured at 29°C for 2-days still successfully progressed into flies. However, *Act5C*^{RNAi} cultures maintained at 29°C for the initial 3-days began displaying varying degrees of arrested larval development and pupal necrosis, though some still progressed into flies, indicating Act5C may be functionally required during the post-L1 stages of larval development (**Figure 6A**). Extending our 29°C treatment for 4-days resulted in progressively fewer larvae able to develop into flies, and 5-days at 29°C resulted in the developmental arrest and necrotic pupae observed with constitutive Act5C depletion (**Figure 6A**). Collectively, this indicates that Act5C is not essential for embryogenesis but is required for post-embryonic larval development.

To further dissect the developmental time-period at which Act5C is required, we monitored *Act5C*^{RNAi} larvae hatched and maintained at the permissive 18°C, then later transferred to the non-permissive 29°C at different ages. Because 18°C incubation has been shown to predictably slow embryonic and larval developmental times by a factor of two (Ashburner et al., 2005; Shellenbarger and Mohler, 1978; Yadav and Sharma, 2013), an adjusted developmental timespan that accounts for this delay was employed. Thus, embryogenesis at 18°C actually requires two “real” days (denoted here as 1 “adjusted development day”, or 1-day*). Intriguingly, when cultures were initially placed at the permissive 18°C for only 0.5-day* or 1-day*, then switched to non-permissive 29°C, larvae exhibited developmental arrest and failed to generate flies, suggesting that Act5C expression in the FB *only* during embryogenesis is *not* sufficient for complete *Drosophila* development (**Figure 6B**). This again supports a model where Act5C is functionally important in the post-embryonic larval stages of development. Next, we extended

the permissive 18°C treatment for 1.5-days*, and observed a small, but variable (≤30%) proportion of flies hatching across several culture vials analyzed. Further extension to 2-days* at 18°C enabled ~70% of pupae to eclose to flies (**Figure 6B**). An almost complete rescue was noted with vials maintained for 2.5-days* at 18°C. Collectively, both Gal80ts temperature-shift experiments suggest that Act5C is functionally important *after* embryogenesis and during the L1-L3 larval stages of development when the FB tissue is rapidly expanding. During this developmental period, larvae are actively feeding, growing, and storing dietary nutrients derived from the gut in the FB, which requires inter-organ lipid trafficking and signaling to coordinate nutrient storage and FB tissue growth.

To further dissect the developmental time-window when Act5C was required, we took advantage of previous studies showing that simply maintaining *Drosophila* stocks at lower temperatures can limit the degree of RNAi-mediated protein depletion in UAS-TRiP/Gal4 systems, even without the involvement of Gal80 (Duffy, 2002; Perkins et al., 2015). Indeed, we observed that while FBs of *Dcg-Gal4>UAS-Act5C*^{RNAi} larvae maintained at 25°C throughout development did not contain a cortical actin network (phalloidin-stained), those maintained at 18°C exhibited a partial F-actin network, indicating some Act5C was still present at this cooler temperature (**Figure 6C, red arrows**). Furthermore, larvae constitutively maintained at 18°C were generally larger and successfully developed into flies, whereas those maintained at 25°C exhibited developmental arrest and pupal necrosis, indicating that at 18°C Act5C was expressing above its functional threshold (**Figure 6D,E**). The *Act5C*^{RNAi} larvae cultured at 18 °C also displayed improved FB tissue morphology and normal FB cell sizes (**Figure 6D,F**).

Equipped with this additional temperature-sensitive experimental approach, we queried how culturing *Dcg-Gal4>UAS-Act5C*^{RNAi} at the optimal laboratory rearing temperature of 25°C (Ashburner et al., 2005; Merkey et al., 2011) during egg-laying and early development (Act5C^{OFF}), then switching to 18°C at which RNAi efficiency is considerably reduced (Act5C^{functional}), would impact larval development. Like the Gal80ts system, maintaining cultures for 1-day at 25°C, then switching to 18°C still permitted full development into flies, again indicating that Act5C was not functionally required during embryogenesis (**Figure 6G**). Extending the 25°C timeframe to 2-days still allowed fly development, whereas 3-days at 25°C led to developmental arrest and necrotic pupae similar to continually maintaining them at this temperature (**Figure 6G**). This further supports a model where Act5C is not functionally

necessary during embryogenesis but is required later during larval development. Finally, we monitored *Dcg-Gal4>Act5C*^{RNAi} cultures initially reared at 18°C then transitioned to 25°C. Again, similar to the Gal80ts system, cultures kept at 18°C for 1-day* (Act5C expressed during embryogenesis only) failed to develop into flies, whereas some larvae from cultures maintained at 18°C for 1.5-days* could successfully complete metamorphosis into flies (**Figure 6H**). Cultures maintained for the initial 2.5-days* at 18°C completed normal development into flies, underscoring that expressing Act5C only during embryogenesis is not sufficient for full development, but rather Act5C is required during the feeding phases of larval growth and development.

Act5C is required for FB cell size expansion during larval development

Given that larvae are actively feeding and growing during the L1-L3 developmental time window, and adipocytes in *Act5C*^{RNAi} developmentally arrested larvae were small, we hypothesized that Act5C may be required for the physical expansion of FB cells and tissue during larval feeding and development. FB tissue expands by increasing individual cell size but not cell number, and this growth is necessary to accommodate the vast amounts of lipids and general biomass necessary for achieving 'critical weight' and successful progression through metamorphosis (Merkey et al., 2011; Tennessen and Thummel, 2011). Indeed, our hypothesis is also supported by work in mice suggesting that drastic actin reorganization is required to expand adipocyte cell sizes during high-fat diets (Hansson et al., 2019). Reinforcing this, our imaging revealed cortical actin networks at cell-cell boundaries within FB tissues, apart from hemolymph-exposed surfaces, implying such intra-tissue actin assemblies may be dedicated more to cell ultra-structural support and growth, rather than Lpp secretion into the hemolymph.

To begin, we examined whether F-actin turnover was required for normal FB cell size in larval development. We quantified the areas of FB cells from age-matched pre-wandering control larvae and those with FB-specific Twf depletion (*Dcg-Gal4>UAS-Twf*^{RNAi}). Indeed, we found that interfering with F-actin turnover led to significantly decreased FB cell size in *Twf*^{RNAi} FBs, similar to Act5C loss (**Figure 2M, Figure 7A**). In contrast, FB-specific RNAi depletion of beta-spectrin did not reduce FB cell size, and in fact FB cells were very slightly larger than controls. This indicated that F-actin turnover was required for FB cells to achieve normal size during larval development.

Next, we again employed the GAL80ts system to dissect how temporally altering Act5C expression in the FB impacted FB cell size just prior to pupation. We quantified FB cell sizes of pre-wandering L3 larvae cultured at the permissive 18°C ($Act5C^{ON}$) for the initial 1.5-days*, then moved to 29°C (non-permissive, $Act5C^{OFF}$) for the remainder of larval development. Of note, this 1.5-day* temperature scheme enables only a few larvae to successfully develop into flies (**Figure 6B, Figure 7B**). These larvae exhibited significantly smaller FB cells, indicating that loss of Act5C expression after only 1.5-days* suppressed FB cell growth during larval development (**Figure 7B**). Next, we examined FBs from larvae cultured initially at 18°C for 2-days* or 2.5-days* (followed by Act5C silencing at 29°C), which in the previous experiments enabled a majority of larvae to develop into flies. Indeed, the 2-days* larvae exhibited normal-sized FB cells, and surprisingly the 2.5-days* larvae exhibited slightly larger FB cells than controls (**Figure 7B**). These experiments collectively indicate that Act5C expression during larval growth is required for normal FB cell enlargement and correlates with successful development.

To query how these time-specific experiments related to FB TG storage, we also measured larval TG levels of L3 pre-wandering larvae. There was a direct correlation between smaller FB cells and reduced TG storage; larvae from cultures kept at 18°C for the initial 1-day* or 1.5-days* displayed significantly less TG than controls. TG levels successively increased with longer times at the permissive temperature, i.e. 2-day* and 2.5-day* (**Figure 7C**). Collectively, this supports a model where Act5C is required for FB cell size expansion as well as TG storage during the feeding phases of larval development.

Next, we examined FB cell sizes and TG levels of larvae from cultures initially maintained at the non-permissive 29°C temperature ($Act5C^{OFF}$). Loss of Act5C during embryogenesis only (1-day at 29°C) did not significantly impact FB cell sizes of pre-wandering L3 larvae, and their TG levels mirrored controls (**Figure 7D,E**). This is consistent with their ability to develop into flies. However, extension of this non-permissive 29°C to 3-days and 5-days caused progressive reductions in both FB cells size and TG stores in the L3 non-wandering larvae (**Figure 7D,E**). Collectively, this indicates that Act5C is required for FB cell size expansion and TG stores, specifically in the post-embryonic phases of larval development.

As a final question, we queried whether Lpp particles were required for normal larval FB cell size. We quantified FB cell sizes of synchronized control L3 non-wandering larvae and those

with stable RNAi-silencing of Lpp (*Dcg-Gal4>ApoLpp*^{RNAi}). Indeed, Lpp loss significantly reduced FB cell size similar to Act5C loss (**Figure 7F**). This suggests that Lpp trafficking/signaling is also required for normal FB cell size. This collectively supports a model where Act5C is required for Lpp secretion and associated inter-organ signaling, but may in parallel also be necessary for structural support and cytoskeletal dynamics at intra-cellular interfaces to coordinate FB cell expansion with nutrient accrual during the larval feeding stages prior to metamorphosis (**Figure 7G**).

Discussion

The actin cytoskeleton is an essential scaffold for cell integrity and plays roles in organelle homeostasis as well as organismal growth and development (Hansson et al., 2019; Ojelade et al., 2013). In mammals, adipocyte differentiation, formation, and expansion require actin network remodeling, and defects in actin-associated processes are associated with metabolic diseases like type 2 diabetes (Hansson et al., 2019; Kim et al., 2019). Clear knowledge gaps remain regarding how actin influences nutrient uptake, storage, and adipocyte cell size. Here, we dissected how the cortical actin network of *Drosophila* larval FB cells influences nutrient trafficking and storage, as well as how it contributes to biomass accruement during larval development. We find that Act5C plays an essential role in post-embryonic larval growth and inter-organ lipid trafficking. Moreover, we mechanistically reveal that Act5C is required for the cortical actin meshwork that shapes the FB cell surface. Surprisingly, loss of this actin network does not reduce the ability of FB cells to absorb carbohydrates nor lipids, but rather perturbs FB release of Lpp particles, which mediate lipid trafficking from the gut to the FB and other organs. We also find that post-embryonic loss of Act5C specifically in the FB perturbs adipocyte tissue expansion, thereby hampering nutrient accumulation, leading to lipodystrophic larvae that are developmentally delayed and unable to complete metamorphosis.

How does Act5C contribute to Lpp secretion and gut:FB nutrient trafficking? We find that the FB actin cytoskeleton closely associates with surface membrane microridges and pLDs, suggesting Act5C influences lipid homeostasis and potentially lipid exchange between the hemolymph and FB cells at the cell surface. In line with this, immuno-staining and TEM reveal Lpp particles cluster adjacent to pLDs, consistent with reports indicating that lipoproteins and LDs are lipidated with TG at common ER sub-domains (Taghibiglou et al., 2000; Ye et al., 2009). Indeed, our previous work revealed that loss of Lpp particles caused drastic alterations in larval

FB pLDs, indicating a functional connection between Lpp and pLDs at the cell surface (Ugrankar et al., 2019). In the tissue interior, Act5C also localizes to cell-cell boundaries. We propose that this Act5C pool may contribute to maintaining tissue architecture as well as promoting cell size expansion during larval feeding and growth. Such cell expansion is necessary to provide FB tissue volume for TG storage and biomass accumulation necessary for achieving larval "critical weight". In support of this, FB-specific Act5C depletion yielded undersized FB cells with smaller and misshapen mLDs. Consequently, larvae suffered from generalized lipodystrophy, reduced overall TG storage and smaller body size relative to age-matched controls. Few Act5C-deficient larvae reached CW for pupation even after a significant delay of 7-14 days. Moreover, *Act5C*^{RNAi} larvae that did pupate became necrotic, presumably because they lacked the energy and/or biomass for adult tissue differentiation. Similar lipodystrophic *Drosophila* models, such as larvae lacking the lipin homolog dLipin, also exhibited undersized FBs containing small LDs, developmental delay, and late pupal lethality as pharate adults (Ugrankar et al., 2011). Thus, the failure of *Act5C*^{RNAi} larvae to complete development suggests that appropriate FB lipid storage and biomass increase during larval feeding stages requires an intact FB cortical actin cytoskeleton.

The cell cortex consists not only of the actin cytoskeleton but also several actin-binding proteins that regulate actin turnover (e.g., Twf), and a spectrin network comprised of alpha- and beta-spectrin that cross-link with F-actin filaments at the cell surface, providing architectural support (Brozinick et al., 2007; Köster and Mayor, 2016). It has been previously shown that loss of alpha- or beta-spectrin eliminates the FB cell surface mircoridges and alters pLD size (Diaconeasa et al., 2013; Ugrankar et al., 2019). While these defects were recapitulated in Act5C^{-}deficient FBs as well, intriguingly loss of actin and spectrins differentially impacted larval lipid homeostasis. Whereas Act5C or Twf loss reduced whole larval TG and hemolymph DAG pools, and increased gut TG levels, loss of beta-spectrin had no effect on any of these. This indicates that the FB cortical actin and spectrin networks, while both localized to the FB cell surface, play distinct roles in tissue homeostasis, with spectrins functioning primarily in surface architectural support, whereas actin contributes more functionally to inter-organ nutrient trafficking and lipid storage.

Larval development can arrest for several reasons, including poor nutrient availability, inefficient delivery to tissues, or defective nutrient storage/utilization (Tennessen and Thummel, 2011). The larval gut absorbs and digests dietary carbohydrates, lipids, and proteins into metabolic

intermediates, which are transported to various organs and tissues through the circulating hemolymph. The FB is the primary site of nutrient uptake and energy storage. Both dietary sugars and fatty acids are assimilated into FB LDs as TG, though some carbohydrates from circulation may be converted to glycogen stores (Musselman and Kühnlein, 2018; Palm et al., 2012; Yamada et al., 2018). In mammals, the adipocyte actin network has been proposed to regulate stimulated Glut4 trafficking to the PM where it can facilitate carbohydrate uptake (Brozinick et al., 2007; Kim et al., 2019). Unexpectedly, we find that Act5C loss does not impact the ability of FB cells to absorb carbohydrates (2-NBD-glucose) or lipids (BODIPY-C12), and we confirm that larvae lacking Act5C in the FBs exhibit normal glycogen stores and circulating sugars. Instead, we find that Act5C is necessary for Lpp secretion and subsequent inter-organ nutrient transport, indicating a non-canonical model by which cortical actin influences adipose tissue nutrient storage. We also find that Act5C-deficient FBs display reduced TG synthesis potential, with decreased *MDY* and *DESAT1* mRNA levels. This may indicate that FB tissue size may transcriptionally influence TG synthesis pathways, and that Act5C-deficient FBs lacking the volume to store TG may down-regulate TG synthesis through signaling. Further studies are needed to understand this crosstalk. Since the FB is functionally analogous to both the mammalian adipose and liver (Arrese and Soulages, 2010; Musselman et al., 2013; Musselman and Kühnlein, 2018), our results suggest that perturbation of actin dynamics in mammalian hepatocytes may also alter lipoprotein secretion, and decrease inter-organ lipid trafficking.

The FB tissue forms during late embryogenesis and its homeostasis is critical for larval development (Hoshizaki et al., 1994; Yongmei Xi, 2015). Using temperature-dependent and temporal genetic manipulation approaches, we made the surprising observation that Act5C is not required during embryogenesis itself, but rather during post-embryonic larval developmental. Loss of Act5C during the feeding larval stages led to smaller larvae and FB cells, as well as reduced whole body TG storage. This collectively supports a model where Act5C is required for post-embryonic FB tissue growth, so the FB can accumulate sufficient energy reserves for metamorphosis. Indeed, previous studies indicate that loss of inter-organ lipid transport (*ApoLpp*) or nutrient signaling (*CK1alpha*) also lead to developmental arrest (Palm et al., 2012; Ugrankar et al., 2015), suggesting shared mechanisms between nutrient sensing/storage and FB cell expansion in biomass accruement. Indeed, ApoLpp-deficient larvae also exhibited smaller FB cells that mirrored Act5C loss, suggesting that the decreased FB cell size in Act5C-depleted larvae may be also through reduced lipid transport or its associated nutrient signaling

pathways. Further studies will dissect this relationship between actin dynamics and Lpp-dependent nutrient signaling in FB tissue growth.

Acknowledgements:

The authors thank members of the Henne and Friedman labs for insights and discussion. We would also like to thank Dr. Anza Darehshouri, Phoebe Doss, and Rebecca Jackson for assistance with TEM. We are also grateful to Dr. Saikat Mukhopadhyay for use of his light and stereo microscopes and Real-Time QPCR machine. W.M.H. is supported by funds from the Welch Foundation (I-1873), the NIH NIGMS (GM119768), NIDDK (DK126887), and the UT Southwestern Endowed Scholars Program.

References

Arrese, E.L., Soulages, J.L., 2010. Insect fat body: energy, metabolism, and regulation. Annu. Rev. Entomol. 55, 207–225. https://doi.org/10.1146/annurev-ento-112408-085356

Ashburner, M., Golic, K.G., Hawley, R.S., 2005. Drosophila: a laboratory handbook, 2nd ed. ed. Cold Spring Harbor Laboratory Press, Cold Spring Harbor, N.Y.

Bharucha, K.N., 2009. The epicurean fly: using Drosophila melanogaster to study metabolism. Pediatr. Res. 65, 132–137. https://doi.org/10.1203/PDR.0b013e318191fc68

Brozinick, J., Berkemeier, B., Elmendorf, J., 2007. “Actin”g on GLUT4: Membrane & Cytoskeletal Components of Insulin Action. Curr. Diabetes Rev. 3, 111–122. https://doi.org/10.2174/157339907780598199

Burn, T.C., Vigoreaux, J.O., Tobin, S.L., 1989. Alternative 5C actin transcripts are localized in different patterns during Drosophila embryogenesis. Dev. Biol. 131, 345–355. https://doi.org/10.1016/s0012-1606(89)80008-9

Crivat, G., Lizunov, V.A., Li, C.R., Stenkula, K.G., Zimmerberg, J., Cushman, S.W., Pick, L., 2013. Insulin stimulates translocation of human GLUT4 to the membrane in fat bodies of transgenic Drosophila melanogaster. PloS One 8, e77953. https://doi.org/10.1371/journal.pone.0077953

Dantuma, N.P., Pijnenburg, M.A.P., Diederen, J.H.B., Van der Horst, D.J., 1998. Multiple interactions between insect lipoproteins and fat body cells: extracellular trapping and endocytic trafficking. J. Lipid Res. 39, 1877–1888. https://doi.org/10.1016/S0022-2275(20)32176-3

De Moed, G.H., Kruitwagen, C.L.J.J., De Jong, G., Scharloo, W., 1999. Critical weight for the induction of pupariation in Drosophila melanogaster: genetic and environmental variation. J. Evol. Biol. 12, 852–858. https://doi.org/10.1046/j.1420-9101.1999.00103.x

Diaconeasa, B., Mazock, G.H., Mahowald, A.P., Dubreuil, R.R., 2013. Genetic studies of spectrin in the larval fat body of Drosophila melanogaster: evidence for a novel lipid uptake apparatus. Genetics 195, 871–881. https://doi.org/10.1534/genetics.113.155192

Duffy, J.B., 2002. GAL4 system in Drosophila: a fly geneticist's Swiss army knife. Genes. N. Y. N 2000 34, 1–15. https://doi.org/10.1002/gene.10150

Hansson, B., Morén, B., Fryklund, C., Vliex, L., Wasserstrom, S., Albinsson, S., Berger, K., Stenkula, K.G., 2019. Adipose cell size changes are associated with a drastic actin remodeling. Sci. Rep. 9, 12941. https://doi.org/10.1038/s41598-019-49418-0

Havula, E., Teesalu, M., Hyötyläinen, T., Seppälä, H., Hasygar, K., Auvinen, P., Orešič, M., Sandmann, T., Hietakangas, V., 2013. Mondo/ChREBP-Mlx-Regulated Transcriptional Network Is Essential for Dietary Sugar Tolerance in Drosophila. PLoS Genet. 9, e1003438. https://doi.org/10.1371/journal.pgen.1003438

Heier, C., Klishch, S., Stilbytska, O., Semaniuk, U., Lushchak, O., 2021. The Drosophila model to interrogate triacylglycerol biology. Biochim. Biophys. Acta Mol. Cell Biol. Lipids 1866, 158924. https://doi.org/10.1016/j.bbalip.2021.158924

Heier, C., Kühnlein, R.P., 2018. Triacylglycerol Metabolism in Drosophila melanogaster. Genetics 210, 1163–1184. https://doi.org/10.1534/genetics.118.301583

Hoshizaki, D.K., Blackburn, T., Price, C., Ghosh, M., Miles, K., Ragucci, M., Sweis, R., 1994. Embryonic fat-cell lineage in Drosophila melanogaster. Dev. Camb. Engl. 120, 2489–2499. https://doi.org/10.1242/dev.120.9.2489

Juarez-Carreño, S., Vallejo, D.M., Carranza-Valencia, J., Palomino-Schätzlein, M., Ramon-Cañellas, P., Santoro, R., de Hartog, E., Ferres-Marco, D., Romero, A., Peterson, H.P., Ballesta-Illan, E., Pineda-Lucena, A., Dominguez, M., Morante, J., 2021. Body-fat sensor triggers ribosome maturation in the steroidogenic gland to initiate sexual maturation in Drosophila. Cell Rep. 37, 109830. https://doi.org/10.1016/j.celrep.2021.109830

Kanzaki, M., Pessin, J.E., 2002. Caveolin-associated filamentous actin (Cav-actin) defines a novel F-actin structure in adipocytes. J. Biol. Chem. 277, 25867–25869. https://doi.org/10.1074/jbc.C200292200

Kasurinen, J., 1992. A novel fluorescent fatty acid, 5-methyl-BDY-3-dodecanoic acid, is a potential probe in lipid transport studies by incorporating selectively to lipid classes of BHK cells. Biochem. Biophys. Res. Commun. 187, 1594–1601. https://doi.org/10.1016/0006-291x(92)90485-4

Kim, J.I., Park, J., Ji, Y., Jo, K., Han, S.M., Sohn, J.H., Shin, K.C., Han, J.S., Jeon, Y.G., Nahmgoong, H., Han, K.H., Kim, J., Kim, S., Choe, S.S., Kim, J.B., 2019. During Adipocyte Remodeling, Lipid Droplet Configurations Regulate Insulin Sensitivity through F-Actin and G-Actin Reorganization. Mol. Cell. Biol. 39, e00210-19. https://doi.org/10.1128/MCB.00210-19

Köster, D.V., Mayor, S., 2016. Cortical actin and the plasma membrane: inextricably intertwined. Curr. Opin. Cell Biol. 38, 81–89. https://doi.org/10.1016/j.ceb.2016.02.021

Liu, L., Jedrychowski, M.P., Gygi, S.P., Pilch, P.F., 2006. Role of insulin-dependent cortical fodrin/spectrin remodeling in glucose transporter 4 translocation in rat adipocytes. Mol. Biol. Cell 17, 4249–4256. https://doi.org/10.1091/mbc.e06-04-0278

Matsuo, N., Nagao, K., Suito, T., Juni, N., Kato, U., Hara, Y., Umeda, M., 2019. Different mechanisms for selective transport of fatty acids using a single class of lipoprotein in Drosophila. J. Lipid Res. 60, 1199–1211. https://doi.org/10.1194/jlr.M090779

McGuire, S.E., Mao, Z., Davis, R.L., 2004. Spatiotemporal gene expression targeting with the TARGET and gene-switch systems in Drosophila. Sci. STKE Signal Transduct. Knowl. Environ. 2004, pl6. https://doi.org/10.1126/stke.2202004pl6

Merkey, A.B., Wong, C.K., Hoshizaki, D.K., Gibbs, A.G., 2011. Energetics of metamorphosis in Drosophila melanogaster. J. Insect Physiol. 57, 1437–1445. https://doi.org/10.1016/j.jinsphys.2011.07.013

Meschi, E., Delanoue, R., 2021. Adipokine and fat body in flies: Connecting organs. Mol. Cell. Endocrinol. 533, 111339. https://doi.org/10.1016/j.mce.2021.111339

Moseley, J.B., Okada, K., Balcer, H.I., Kovar, D.R., Pollard, T.D., Goode, B.L., 2006. Twinfilin is an actin-filament-severing protein and promotes rapid turnover of actin structures in vivo. J. Cell Sci. 119, 1547–1557. https://doi.org/10.1242/jcs.02860

Musselman, L.P., Fink, J.L., Ramachandran, P.V., Patterson, B.W., Okunade, A.L., Maier, E., Brent, M.R., Turk, J., Baranski, T.J., 2013. Role of fat body lipogenesis in protection

against the effects of caloric overload in Drosophila. J. Biol. Chem. 288, 8028–8042. https://doi.org/10.1074/jbc.M112.371047

Musselman, L.P., Kühnlein, R.P., 2018. Drosophila as a model to study obesity and metabolic disease. J. Exp. Biol. 221, jeb163881. https://doi.org/10.1242/jeb.163881

Nijhout, H.F., Williams, C.M., 1974. Control of moulting and metamorphosis in the tobacco hornworm, Manduca sexta (L.): growth of the last-instar larva and the decision to pupate. J. Exp. Biol. 61, 481–491. https://doi.org/10.1242/jeb.61.2.481

Nunn, E.R., Shinde, A.B., Zaganjor, E., 2022. Weighing in on Adipogenesis. Front. Physiol. 13, 821278. https://doi.org/10.3389/fphys.2022.821278

Ojelade, S.A., Acevedo, S.F., Rothenfluh, A., 2013. The role of the actin cytoskeleton in regulating Drosophila behavior. Rev. Neurosci. 24, 471–484. https://doi.org/10.1515/revneuro-2013-0017

Palm, W., Sampaio, J.L., Brankatschk, M., Carvalho, M., Mahmoud, A., Shevchenko, A., Eaton, S., 2012. Lipoproteins in Drosophila melanogaster--assembly, function, and influence on tissue lipid composition. PLoS Genet. 8, e1002828. https://doi.org/10.1371/journal.pgen.1002828

Perkins, L.A., Holderbaum, L., Tao, R., Hu, Y., Sopko, R., McCall, K., Yang-Zhou, D., Flockhart, I., Binari, R., Shim, H.-S., Miller, A., Housden, A., Foos, M., Randkelv, S., Kelley, C., Namgyal, P., Villalta, C., Liu, L.-P., Jiang, X., Huan-Huan, Q., Wang, X., Fujiyama, A., Toyoda, A., Ayers, K., Blum, A., Czech, B., Neumuller, R., Yan, D., Cavallaro, A., Hibbard, K., Hall, D., Cooley, L., Hannon, G.J., Lehmann, R., Parks, A., Mohr, S.E., Ueda, R., Kondo, S., Ni, J.-Q., Perrimon, N., 2015. The Transgenic RNAi Project at Harvard Medical School: Resources and Validation. Genetics 201, 843–852. https://doi.org/10.1534/genetics.115.180208

Röper, K., Mao, Y., Brown, N.H., 2005. Contribution of sequence variation in Drosophila actins to their incorporation into actin-based structures in vivo. J. Cell Sci. 118, 3937–3948. https://doi.org/10.1242/jcs.02517

Sassu, E.D., McDermott, J.E., Keys, B.J., Esmaeili, M., Keene, A.C., Birnbaum, M.J., DiAngelo, J.R., 2012. Mio/dChREBP coordinately increases fat mass by regulating lipid synthesis and feeding behavior in Drosophila. Biochem. Biophys. Res. Commun. 426, 43–48. https://doi.org/10.1016/j.bbrc.2012.08.028

Schönborn, J.W., Jehrke, L., Mettler-Altmann, T., Beller, M., 2019. FlySilico: Flux balance modeling of Drosophila larval growth and resource allocation. Sci. Rep. 9, 17156. https://doi.org/10.1038/s41598-019-53532-4

Schroeder, C.M., Tomlin, S.A., Mejia Natividad, I., Valenzuela, J.R., Young, J.M., Malik, H.S., 2021. An actin-related protein that is most highly expressed in Drosophila testes is critical for embryonic development. eLife 10, e71279. https://doi.org/10.7554/eLife.71279

Shellenbarger, D.L., Mohler, J.D., 1978. Temperature-sensitive periods and autonomy of pleiotropic effects of l(1)Nts1, a conditional notch lethal in Drosophila. Dev. Biol. 62, 432–446. https://doi.org/10.1016/0012-1606(78)90226-9

Suh, J.M., Stenesen, D., Peters, J.M., Inoue, A., Cade, A., Graff, J.M., 2008. An RGS-containing sorting nexin controls Drosophila lifespan. PloS One 3, e2152. https://doi.org/10.1371/journal.pone.0002152

Taghibiglou, C., Carpentier, A., Van Iderstine, S.C., Chen, B., Rudy, D., Aiton, A., Lewis, G.F., Adeli, K., 2000. Mechanisms of hepatic very low density lipoprotein overproduction in insulin resistance. Evidence for enhanced lipoprotein assembly, reduced intracellular ApoB degradation, and increased microsomal triglyceride transfer protein in a fructose-fed hamster model. J. Biol. Chem. 275, 8416–8425. https://doi.org/10.1074/jbc.275.12.8416

Tennessen, J.M., Thummel, C.S., 2011. Coordinating growth and maturation - insights from Drosophila. Curr. Biol. CB 21, R750-757. https://doi.org/10.1016/j.cub.2011.06.033

Ugrankar, R., Berglund, E., Akdemir, F., Tran, C., Kim, M.S., Noh, J., Schneider, R., Ebert, B., Graff, J.M., 2015. Drosophila glucome screening identifies Ck1alpha as a regulator of mammalian glucose metabolism. Nat. Commun. 6, 7102. https://doi.org/10.1038/ncomms8102

Ugrankar, R., Bowerman, J., Hariri, H., Chandra, M., Chen, K., Bossanyi, M.-F., Datta, S., Rogers, S., Eckert, K.M., Vale, G., Victoria, A., Fresquez, J., McDonald, J.G., Jean, S., Collins, B.M., Henne, W.M., 2019. Drosophila Snazarus Regulates a Lipid Droplet Population at Plasma Membrane-Droplet Contacts in Adipocytes. Dev. Cell 50, 557-572.e5. https://doi.org/10.1016/j.devcel.2019.07.021

Ugrankar, R., Liu, Y., Provaznik, J., Schmitt, S., Lehmann, M., 2011. Lipin is a central regulator of adipose tissue development and function in Drosophila melanogaster. Mol. Cell. Biol. 31, 1646–1656. https://doi.org/10.1128/MCB.01335-10

Virtue, S., Vidal-Puig, A., 2010. Adipose tissue expandability, lipotoxicity and the Metabolic Syndrome--an allostatic perspective. Biochim. Biophys. Acta 1801, 338–349. https://doi.org/10.1016/j.bbalip.2009.12.006

Wagner, C.R., Mahowald, A.P., Miller, K.G., 2002. One of the two cytoplasmic actin isoforms in Drosophila is essential. Proc. Natl. Acad. Sci. U. S. A. 99, 8037–8042. https://doi.org/10.1073/pnas.082235499

Wojczynski, M.K., Glasser, S.P., Oberman, A., Kabagambe, E.K., Hopkins, P.N., Tsai, M.Y., Straka, R.J., Ordovas, J.M., Arnett, D.K., 2011. High-fat meal effect on LDL, HDL, and VLDL particle size and number in the Genetics of Lipid-Lowering drugs and diet network (GOLDN): an interventional study. Lipids Health Dis. 10, 181. https://doi.org/10.1186/1476-511X-10-181

Yadav, P., Sharma, V.K., 2013. Correlated changes in circadian clocks in response to selection for faster pre-adult development in fruit flies Drosophila melanogaster. J. Comp. Physiol. [B] 183, 333–343. https://doi.org/10.1007/s00360-012-0716-1

Yamada, T., Habara, O., Kubo, H., Nishimura, T., 2018. Fat body glycogen serves as a metabolic safeguard for the maintenance of sugar levels in Drosophila. Dev. Camb. Engl. 145, dev158865. https://doi.org/10.1242/dev.158865

Yang, K., Liu, M., Feng, Z., Rojas, M., Zhou, L., Ke, H., Pastor-Pareja, J.C., 2021. ER exit sites in Drosophila display abundant ER-Golgi vesicles and pearled tubes but no megacarriers. Cell Rep. 36, 109707. https://doi.org/10.1016/j.celrep.2021.109707

Ye, J., Li, J.Z., Liu, Y., Li, X., Yang, T., Ma, X., Li, Q., Yao, Z., Li, P., 2009. Cideb, an ER- and Lipid Droplet-Associated Protein, Mediates VLDL Lipidation and Maturation by Interacting with Apolipoprotein B. Cell Metab. 9, 177–190. https://doi.org/10.1016/j.cmet.2008.12.013

Yongmei Xi, Y.Z., 2015. Fat Body Development and its Function in Energy Storage and Nutrient Sensing in Drosophila melanogaster. J. Tissue Sci. Eng. 06. https://doi.org/10.4172/2157-7552.1000141

MATERIALS AND METHODS:

Fly Cultures and Strains

Drosophila feeding L3 stage larvae were used for all larval assays. All *Drosophila* animal research was performed in accordance with NIH recommended policies. Flies were reared and maintained on standard fly food containing cornmeal, yeast, molasses (~5% sugars), and agar. The *Dcg-Gal4* fat body (FB)-specific driver, previously described in (Suh et al., 2008), and *Dcg-Gal4;tub-Gal80ts* strains were provided by Jonathan M. Graff (UTSW) respectively. *UAS-*

Act5C^{RNAi} and other TRiP RNAi stocks and protein/organelle marker strains used were obtained from the Bloomington Stock Center (Bloomington, IN). The *UAS-hGlut4-GFP* line was made by BestGene by injecting a UAS plasmid that was a kind gift of Dr. Leslie Pick (University of Maryland). All crosses involving Gal4 and UAS lines were cultured at 25°C to maintain uniform transgene expression, unless otherwise indicated. All RNAi knockdowns were conducted using the Gal4/UAS system.

Fat Body/ Larval Gut Dissection and Staining

Late-feeding L3 larvae were gently removed from inside the food media using a paintbrush and rinsed in water to remove food particles. Fat bodies (FBs) or guts were dissected from larvae in PBS using Dumont #5 forceps (Electron Microscopy Sciences). All tissues were fixed in 4% paraformaldehyde for 20 min at room temperature and rinsed briefly in PBS prior to staining with organelle labeling dyes. Lipid droplets in FBs were stained by incubating FBs in 100 μM monodansylpentane (MDH) LD stain (Abgent) for 30 min at room temperature, in the dark. F-actin structures were stained with Phalloidin (1:400) or CellMask Green Actin Tracking Stain (1:1000) according to manufacturer's instructions (Invitrogen). LDs in guts were stained with 1 μM Nile Red for 30 min at room temperature, in the dark. Next, FBs and guts were rinsed in PBS and mounted on slides in SlowFade Gold antifade reagent with DAPI (Invitrogen) for subsequent imaging.

Temperature-shift Experiments using tub-Gal80ts

Mated flies (*Dcg-Gal4;tub-Gal80ts X UAS-Act5C*^{RNAi}) were allowed to lay eggs for 8 hours at 18°C (permissive temperature) or 4 hours at 29°C (nonpermissive temperature) and allowed to develop for 1/2/3/4/5 days before moving culture vial from 18° to 29°C or vice versa for the remainder of fly development. Developmental progress was closely monitored on a daily basis, and larvae from both temperature-shift set-ups were harvested on different days for FB dissection/ confocal microscopy (MDH, phalloidin), and TG measurements by TLCs.

***Drosophila* Tissue Immunofluorescence**

FBs dissected from larvae were fixed in 4% paraformaldehyde at room temperature for 30 min on a nutator, then washed 4 times with 1 X PBST (PBS in 0.1% Tween), 10 min each. Tissues were blocked in 1 X PBST + 2% normal goat serum for 2 hours at room temperature, then incubated with Rb-ApoII primary antibody (1:500 dilution) added to the blocking buffer, overnight at 4°C (ApoII Ab was made by Suzanne Eaton, provided by Akhila Rajan). Next, FBs were

washed 4 times with 1 X PBST 15 min each, followed by incubation with anti-rabbit Alexa546 secondary antibody in blocking buffer (1:1000 dilution) at room temperature in the dark for 2 hours on a nutator. FBs were rinsed again 4 times in 1 X PBST 15 min each, and subsequently mounted in SlowFade Gold antifade reagent with DAPI. Fluorescent structures were observed and imaged by confocal microscopy using standard RFP channel filter at 1 μm step-sizes.

Confocal Fluorescence Microscopy

Prepared slides were imaged using Zeiss LSM880 inverted laser scanning confocal microscope. Tissues stained with organelle dyes and those expressing transgenic fluorescent-tagged proteins (e.g., *UAS-mcd8-GFP, UAS-Act5C-RFP, UAS-hGlut4-GFP*) were imaged using the appropriate channel filter DAPI/RFP/GFP. Most FBs were imaged using a 40X oil immersion objective, as 1 um z-stack sections, or at lower magnification using a 10X objective. Larval guts were imaged using a 20X objective.

Epifluorescence and other Light Microscopy

Whole larvae whose FBs were illuminated by FB-expressing fluorescent-GFP markers were imaged using EVOS FL Cell Imaging System (ThermoFisher) at low 2.5x magnification. Pupal imaging was performed on Leica S8AP0 stereoscope.

Thin Layer Chromatography (TLC)

Larvae were weighed, then homogenized in 2:1:0.8 of methanol:chloroform:water. Samples were incubated in a 37°C water bath for 1 hour. Chloroform and 1M KCl (1:1) were added to the sample, centrifuged at 3000 rpm for 2 min, and the bottom layer containing lipids was aspirated using a syringe. Lipids were dried using argon gas and resuspended in chloroform (100 μl of chloroform/7mg of fly weight). Extracted lipids alongside serially diluted standard neutral lipids of known concentrations were separated on TLC plates using hexane:diethyl ether:acetic acid solvent (80:20:1, v/v/v). TLC plate was air dried for 10 min, spray stained with 3% copper (II) acetate in 8% phosphoric acid and incubated at 145°C in the oven for 30 min to 1 hour to allow bands to develop for scanning and imaging. Neutral lipid (TAG and DAG) band intensity was quantified using Fiji/ImageJ software, and lipid concentrations were calculated from the standard curve generated with standard mixture. In the case of dissected larval guts, dried lipids for all samples were re-suspended in 120 μl of chloroform and final lipid concentrations were calculated by normalizing to protein in sample, measured by standard Bradford assay. Hemolymph (4 μl/sample) for DAG measurements collected from larvae was diluted in 0.1% N-

Phenylthiourea (Sigma-Aldrich) in 50 μl PBS. The same lipid extraction protocol was followed, dried lipids were re-suspended in 75 μl of chloroform, and equal volumes were loaded on TLC plates.

Quantitative PCR

Whole RNA was extracted from FB tissues using Trizol reagent (Ambion Life Technologies) according to manufacturer's instructions. RNA was quantified by Denovix spectrophotometer, and 1 mg of RNA was reverse transcribed to cDNA using ReadyScript cDNA Synthesis Mix (Sigma). QPCR was performed with cDNA and SYBR Green JumpStart TAQ ReadyMix on the BioRad CFX96 Real-Time System; mRNA expression data were normalized to that of the fly housekeeping gene *rp49*. Primer sequences for all transcripts amplified are available upon request.

Transmission Electron Microscopy

FB tissue was removed from *Drosophila* larvae, fixed in 2.5% (v/v) glutaraldehyde in 0.1 M sodium cacodylate buffer paraformaldehyde, and processed in the UT Southwestern Electron Microscopy Core Facility. They were post-fixed in 1% osmium tetroxide and 0.8% K3[Fe(CN6)] in 0.1M sodium cacodylate buffer for 1 hour at room temperature. Cells were rinsed with water and en bloc stained with 2% aqueous uranyl acetate overnight. Next, they were rinsed in buffer and dehydrated with increasing concentration of ethanol, infiltrated with Embed-812 resin and polymerized in a 60°C oven overnight. Blocks were sectioned with a diamond knife (Diatome) on a Leica Ultracut UCT (7) ultramicrotome (Leica Microsystems) and collected onto copper grids, post stained with 2% aqueous uranyl acetate and lead citrate. Images were acquired on a JOEL 1400 Plus transmission electron microscope using a voltage of 120 kV.

2-NBD-Glucose (2-NBDG) and BODIPY-C12 Uptake Assays

FB tissues dissected from L3 larvae starved in PBS for 4 hours (or FB tissues extracted from feeding 3L and pre-incubated in PBS for 4 hours) to deplete glycogen stores, was incubated in 300 μM of a fluorescently labeled glucose analog 2-NBDG (2-Deoxy-2-[(7-nitro-2,1,3-benzoxadiazol-4-yl)amino]-D-glucose) (Sigma-Aldrich, #72987) for 45 min at room temperature, in the dark. FBs were then washed with PBS, fixed in 4% paraformaldehyde for 20 min, washed again in PBS, and mounted in SlowFade on slides. 2-NBDG was imaged using the GFP channel filter by confocal microscopy. To measure BODIPY-C12 uptake, FB tissues from feeding L3 larvae were incubated in BODIPY™ FL C12 (4,4-Difluoro-5,7-Dimethyl-4-Bora-

3a,4a-Diaza-s-Indacene-3-Dodecanoic Acid) (Invitrogen, #D3822) 1:1000 in PBS for 20 min at room temperature, in the dark. Subsequent to fixation with 4% paraformaldehyde, FBs were also stained with MDH LD dye to visualize if BODIPY-C12 was incorporated into LDs. Prepared slides were imaged using DAPI(MDH), and RFP(BODIPY-C12) channel filters on the confocal microscope. Both 2-NBDG and BODIPY-C12 FB cell fluorescence was quantified using the Fiji/Image J software.

Hemolymph Glucose and Trehalose Assays

Feeding larvae washed out from culture vials were collected in 630 μm mesh-fitted baskets (Genesee) and rinsed to get rid of adherent food particles. Larvae were dried and divided onto into piles (10–12 larvae each) on a strip of parafilm. Larvae were bled by tearing the cuticle with Dumont 5 forceps (Electron Microscopy Sciences). Two ul of colorless hemolymph was aspirated from each pile and separately transferred to 96-well plates (Thermo-Scientific) containing 0.1% N-Phenylthiourea (Sigma-Aldrich) in 50 μl PBS. 150 μl of Autokit Glucose reagent (Wako) was added to each well and incubated at room temperature for 20 min before measuring absorbance at 505 nm. Glucose concentration was calculated from a standard curve generated with manufacturer's glucose standards. For trehalose assays, 8 μl of dilute hemolymph was treated with 5 μl of (diluted 8X) porcine kidney trehalase (Sigma) overnight at 37 °C. Ten μl of treated sample was assayed for trehalose as described for glucose.

Glycogen Assay

Dissected FBs were homogenized in 300 μl ice-cold PBS using sonication followed by a syringe (29G1/2 needle). After reserving 20 ul of the homogenate for protein Bradford quantification, the rest of the homogenate was heat inactivated at 70°C for 10 min. Homogenate was then centrifuged at maximum speed at 4°C for 10 min and supernatant was collected in a new tube. In a 96-well plate, 30 μl of each sample was loaded in duplicate rows. Then, 100 μl of Autokit Glucose reagent + amyloglucosidase (1 μl amyloglucosidase {Sigma A1602; 25mg} per 1 ml of Glucose reagent) was added to one row of samples, and 100 μl of Glucose reagent alone (without amyloglucosidase) was added to the duplicate row of samples, and to the glucose standards. The plate was incubated at 37°C for 30 min, after which color intensity was measured using a microplate reader at 505 nm. Free glucose concentration in treated and untreated samples was calculated based on the glucose standard curve. Glycogen concentration (as free glucose) was determined by subtracting glucose in the untreated samples

from those treated with amyloglucosidase. Finally, total glycogen was normalized to protein measured by the Bradford assay.

Fat Body Glycogen Staining

Glycogen in FB tissues was stained using the Periodic Acid-Schiff (PAS) kit (Sigma). Larval FBs were dissected in 1% BSA in PBS, fixed with 4% paraformaldehyde in PBS for 20 min, and washed twice with 1% BSA in PBS. FBs were then incubated in 0.5% period acid solution for 5 min, washed twice with 1% BSA in PBS, then stained with Schiff's reagent for 15 min, washed again, and mounted on slides. PAS stained FB tissues were imaged using the Leica DM6B light microscope.

Mammalian Cell Culture

Huh7 cells were cultured in DMEM (Corning; 10-017-CV) supplemented with 10% Fetal calf serum (Corning; 35-010-CV) and 1% penicillin streptomycin solution (Corning; 30-002- Cl). To induce lipid droplet biogenesis, cells were incubated with 600 μM of Oleic acid (Sigma Aldrich; O1008) conjugated with 100 μM of fatty acid-free BSA (Sigma-Aldrich; A3803) for 16 hours.

Mammalian Cell Immunofluorescence (IF) Staining and Confocal Microscopy

After OA treatment, the cells were fixed with 4% paraformaldehyde solution in PBS for 15 min at room temperature. For IF staining, fixed cells were washed with 1x PBS and permeabilized with 0.1% Triton X-100 in 1X PBS at RT for 5 min. The permeabilized cells were blocked in IF buffer (PBS containing 3% BSA and 0.1% Triton X-100) for 30 min. The cells were then incubated with primary antibody in IF buffer for 1 hour and washed thrice with PBS. This was followed by incubation with secondary antibody in IF buffer for 30 min and three washes with PBS. The primary antibodies used are goat anti-Apolipoprotein B (1:200; Rockland Immunochemicals, Inc; 600-101-111), and mouse anti-Hsp90B1 (1:100; Sigma Aldrich; AMAb91019). The secondary antibodies are donkey anti-mouse AF594 (ThermoFisher Scientific; R37115), and donkey anti-goat AF488 (ThermoFisher Scientific; A11055) used at a dilution of 1:400. Visualization of LDs were achieved by staining the cells with MDH (1:1,000; Abgent; SM1000a) for 15 min at room temperature. The images of the cells were taken using a 63X oil-immersion objective in a laser scanning confocal Zeiss LSM880 + Airyscan microscope. Fiji/ImageJ was used for the representation and quantification of images.

Image Analysis and Quantification

Fiji/ImageJ was used for quantifications involving size of FB lipid droplets and area of larval fat cells imaged by confocal microscopy. First, the area was measured for the entire field of view or a region-of-interest (ROI) of defined size. For lipid droplets (LDs), prior to converting image to binary, a 'smooth' function was applied to the image to remove inherent graininess of the lipid stain and allow for more accurate quantification of LD cross-sectional area. The method for binary conversion was selected based on which one best represented LDs in the region of interest. 'watershed' was performed on binary images, and 'analyze particles' was used to quantify LD number and size. For obtaining fat cell area, the 'polygon selections' tool was used to draw boundaries around individual cells highlighted by fluorescent protein-tagged markers (e.g., phalloidin, CellMask, mcd8-GFP, hGlut4-GFP), and 'analyze', 'measure area' functions were applied. All volumetric analysis and multi-color linescans were conducted using Fiji/ImageJ software.

Statistical Analysis

All experiments were conducted at least 3 times to provide experimental rigor. For the figures, all Comparative statistics were either student t-tests or ANOVA tests for multiple data point experiments. Statistical significance was applied if $p<0.05$. Error bars indicate SD. In general a single * indicates $p<0.05$, ** indicates $p<0.005$, and *** indicates $p<0.0005$.

DATA AND CODE AVAILABILITY

Original/source data for all figures in this paper are available upon request.

Figure Legends:

Figure 1: Act5C forms a cortical actin network at the surfaces of fat body cells.

A) Confocal images of L3 larval fat bodies (FBs) at their mid-plane or periphery stained with phalloidin and Fire-LUT pseudo-colored (Fiji). Scale Bar 10µm.

B) Confocal images of L3 larval FB periphery (*top*) or mid-plane (*bottom*) sections stained with Cell Mask™ Actin Tracking Stain (green) and LD stain monodansylpentane (MDH, magenta). Red arrows mark peripheral LDs (pLDs) encircled by cortical actin. (*bottom right*) A side yz-axis profile of the z-section of the FB tissue, marking pLDs encircled by actin (red arrows). Scale Bar 10µm.

C) Larval control FBs stained with phalloidin and viewed from periphery or mid-plane. Scale bar 10µm.

D) Larval FB expressing *Dcg-Gal4>UAS-Act5C-GFP* and with stained LDs (MDH). Scale Bar 10μm.

E) Larval FB expressing PM marker mCD8-GFP and Act5C-RFP on *Dcg-Gal4*, and with LD stain MDH. Red arrows indicate pLDs encircled by Act5C-RFP. Scale Bar 10μm.

Figure 2: FB-specific Act5C loss perturbs LDs and reduces triglyceride stores

A) Larval FBs from control (*Dcg-Gal4*) or *Dcg-Gal4>Act5C*^{RNAi} and stained for LDs (MDH). Scale Bar 10μm.

B) Comparative chart of average pLD and mLD sizes from FB-specific RNAi depletions of six different Actins compared to control LDs. *Act5C* loss significantly altered pLDs and mLDs compared to *Dcg-Gal4* control.

C) Average pLD sizes (μm^2) for control and FB-specific RNAi actin depletions.

D) Average mLD sizes (μm^2) for control and FB-specific RNAi actin depletions.

E) Total triglycerides for age-matched *control* and *Act5C*^{RNAi} 6-day larvae, and developmentally delayed *Act5C*^{RNAi} 21-day larvae.

F) Q-PCR from isolated larval FBs of lipogenesis and lipolysis related genes.

G) Inverted fluorescent image of age-matched L3 pre-wandering control and *Act5C*^{RNAi} larvae expressing UAS-GFP in their FBs.

H) Vials with control or *Act5C*^{RNAi} pupae. Red arrow denotes necrotic pupae.

I) Age-matched control and *Act5C*^{RNAi} culture vials, showing wandering 3L and pupae in controls at ~day 6 post-laying, but no wandering of *Act5C*^{RNAi} due to developmental delay.

J) Comparison of control and *Act5C*^{RNAi} maturing pupae. Necrotic pupae marked. Scale bar 1mm.

K) Fluorescence micrograph of L3 wandering larvae expressing soluble GFP in the FB (*Dcg-Gal4>UAS-GFP*). Larvae are either control (top) or also FB-depleted Act5C (*Dcg-Gal4>Act5C*^{RNAi}, bottom), latter has a smaller FB and experienced developmental delay prior to wandering (green). Scale bar 2000μm.

L) Fluorescence images of extracted larval FBs from *control* or *Act5C*^{RNAi}. Scale bar 10 μm. FBs stained with LD stain MDH.

M) Average cell size for larval FBs from *control* and *Act5C*^{RNAi}.

N) Representative fluorescent images of LD larval FBs expressing surface marker hGlut4-GFP to illustrate smaller cell size in *Act5C*^{RNAi}. Scale bar 10μm.

Figure 3: The cortical actin and spectrin networks differentially influence FB LDs

A) Cartoon schematic of FB cortical actin and spectrin networks.

B) Confocal sections of larval FBs with periphery (*top*) or mid-plane (*bottom*) stained for LDs (MDH). Control (*Dcg-Gal4*) and *Dcg-Gal4*>RNAi depletion of actin-associated (Act5C, Twf) or spectrin (alpha-spectrin, beta-spectrin) factors are indicated. Scale bar 10μm.

C) Average pLD sizes (μm^2) for FB-specific RNAi depletions compared to controls.

D) Average mLD sizes (μm^2) for FB-specific RNAi depletions compared to controls.

E) Relative whole-larval TG levels compared to controls for different FB-specific RNAi lines.

F) Confocal images (Fire-LUT) of phalloidin-stained larval FBs from *Dcg-Gal4* control or *Dcg-Gal4>Twf*^{RNAi}. Scale bar 10μm.

G) Confocal images of larval FBs expressing surface marker mCD8-RFP (*Dcg-Gal4>UAS-mCD8-RFP*) and stained for LDs (MDH). (*top*) View of the cell periphery LD stain. (*bottom*) Side profile of cell periphery showing mCD8-RFP surface and LD stain. Red arrows indicate small pLDs wrapped by mCD8-RFP surface membrane; this wrapping is lost in either *beta-spectrin*^{RNAi} or *Act5C*^{RNAi}.

Figure 4: Loss of Act5C does not reduce the ability of FBs to absorb carbohydrates or lipids

A) Cartoon of 2-NBD-glucose (2-NBDG) carbohydrate uptake assays using extracted larval FBs.

B) Inverted-LUT fluorescence confocal image of 2-NBD-glucose-exposed larval *Dcg-Gal4* control and *Dcg-Gal4>Act5C*^{RNAi} FBs.

C) Quantification of 2-NBDG average intensities in larval FBs as in B. Scale bar 10μm.

D) Cartoon of BODIPY-C12 fatty acid uptake assays using extracted larval control and *Act5C*^{RNAi} FBs.

E) Inverted-LUT fluorescence confocal image of BODIPY-C12 exposed larval FBs. LD are also stained with MDH. Scale bar 10μm.

F) Quantification of BODIPY-C12 average intensities in larval FBs as in E.

G) Larval hemolymph glucose levels (mg/dL) from control or *Act5C*^{RNAi} larvae.

H) Larval hemolymph trehalose levels (mg/dL) from control or *Act5C*^{RNAi} larvae.

I) Isolated larval FB glycogen levels from control or *Act5C*^{RNAi} larvae.

J) Periodic acid-Schiff (PAS) glycogen stain of larval FBs from control or *Act5C*^{RNAi} larvae.

K) Confocal images of larval FBs expressing *Dcg-Gal4>UAS-hGlut4-GFP* at cell surfaces. Scale bar 10μm.

Figure 5: Act5C loss alters lipoprotein (Lpp) secretion from the FB and gut:FB inter-organ transport

A) Cartoon of lipoprotein (Lpp)-mediated mid-gut:FB inter-organ lipid transport, as well as Lpp secretion out of FB cells via a Sar1/Tango1-dependent secretory pathway.

B) Larval mid-guts stained with Nile Red from *Dcg-Gal4* control and *Dcg-Gal4*>RNAi knock-down of several genes. Scale bar 10μm.

C) Relative TG levels in the larval mid-gut for control and FB-specific RNAi knockdown of several genes.

D) Relative hemolymph diacylglycerol (DAG) levels for control and FB-specific RNAi knock-down of several genes.

E) Confocal immuno-fluorescence of control and *Act5C*^{RNAi} larval FBs stained for lipoprotein (anti:Lpp) and imaged through tissue mid-plane. Red arrows indicate Lpp punctae adjacent to LDs (denoted by negative space). Scale bars: (*left*) 10μm, (*center, right*) 2μm.

F) Transmission electron micrographs (TEM) of larval FBs from control, *Act5C*^{RNAi}, or *ApoLpp*^{RNAi} larvae. Red arrows indicate ~60nm diameter Lpp-like particles, which are absent in *ApoLpp*^{RNAi} FB. Scale bars: 2μm.

Figure 6: Act5C is required during post-embryogenesis larval development

A) Schematic of Gal80 temperature sensitive (Gal80ts) experiments (*Dcg-Gal4;tub-Gal80ts>Act5C*^{RNAi}): 29°C to 18°C switch. *Drosophila* egg-laying occurs at 29°C (maximal Act5C silencing, Act5C^{OFF}), and cultures are maintained at this non-permissive temperature for set time-periods, then transitioned to permissive 18°C to allow Act5C expression for the rest of development (Act5C^{ON}). Their developmental fate (i.e., arrest/necrosis or successful fly eclosion) is indicated. Timeline indicated at bottom. E: embryogenesis, L1, L2, L3: larval developmental stages. W: wandering, P: pupation.

B) Schematic of Gal80ts experiments: 18°C to 29°C switch. *Drosophila* egg-laying occurs at 18°C (Act5C is expressed in the FB). Vials are then maintained at this permissive temperature for set time-periods, then transitioned to non-permissive 29°C to maximally RNAi-silence Act5C expression for the rest of development. Their developmental fate (i.e., arrest/necrosis or successful fly eclosion) is indicated. Timeline indicated at bottom. E: embryogenesis, L1, L2, L3: larval developmental stages. W: wandering, P: pupation.

C) Phalloidin (Fire-LUT)-stained FBs from control, or *Act5C*^{RNAi} larvae cultured at 25°C (efficient RNAi-silencing) or 18°C (inefficient RNAi silencing). Red arrows indicate a cortical actin network from Act5C expression. Scale bar 10µm.

D) Inverted fluorescence image of age-matched L3 non-wandering larvae expressing *UAS-GFP* in FBs. Control, *Act5C*^{RNAi} at 25°C, and *Act5C*^{RNAi} at 18°C are displayed.

E) Schematic of time-lapse experiments in *Dcg-Gal4>Act5C*^{RNAi} vials cultured at either 25°C (enables efficient Act5C RNAi-silencing) or 18°C (some Act5C is expressed due to inefficient RNAi-silencing, Act5C^{functional}). Act5C^{RNAi} larvae maintained throughout at 18°C successfully develop into flies whereas those at 25°C do not.

F) FB cell sizes for L3 non-wandering *Dcg-Gal4* control and *Dcg-Gal4>Act5C*^{RNAi} larvae cultured at 25°C or 18°C.

G) Schematic of *Dcg-Gal4>Act5C*^{RNAi} (25°C to 18°C) temperature-shift experiments. *Drosophila* eggs are laid and cultures maintained at 25°C (for efficient Act5C silencing) for set time-periods, then transitioned to 18°C to permit low Act5C expression but above a functional threshold. Their developmental fate (as in A and B) is indicated. Timeline indicated at bottom. E: embryogenesis, L1, L2, L3: larval developmental stages. W: wandering, P: pupation.

H) Schematic of *Dcg-Gal4>Act5C*^{RNAi} (18°C to 25°C) temperature-shift experiments. *Drosophila* eggs are laid and cultures maintained at 18°C (for low Act5C expression) for set time-periods, then transitioned to 25°C for efficient Act5C RNAi-silencing. Their developmental fate (as in A, B, and G) is indicated. Timeline indicated at bottom. E: embryogenesis, L1, L2, L3: larval developmental stages. W: wandering, P: pupation.

Figure 7: Post-embryonic larval Act5C expression is necessary for FB cell size expansion

A) FB cell sizes for *Dcg-Gal4* control and *Dcg-Gal4>Twf*^{RNAi} and *beta-spectrin*^{RNAi} (via *Dcg-Gal4*) L3 pre-wandering larvae.

B) FB cell sizes for *Dcg-Gal4* control and *Dcg-Gal4;tub-Gal80ts>Act5C*^{RNAi} larvae from 18°C-to-29°C temperature shift experiments, as in Figure 6. The number of days larvae are cultured at the permissive (Act5C^{ON}) 18°C before switching to non-permissive 29°C are denoted.

C) Relative changes in TG for control and Gal80ts 18°C-to-29°C temperature shifted larvae (experiments as in Figure 6). The number of days larvae are cultured at the permissive (Act5C^{ON}) 18°C before switching to non-permissive 29°C are denoted. How these values correlate to FB cell size and development into flies is also noted.

D) FB cell sizes for *Dcg-Gal4* control and *Dcg-Gal4;tub-Gal80ts>Act5C*^{RNAi} larvae from 29°C-to-18°C temperature shift experiments, as in Figure 6. The number of days larvae are kept at the non-permissive (Act5C^{OFF}) 29°C before switching to permissive 18°C are denoted.

E) Relative changes in TG for control and Gal80ts 29°C-to-18°C temperature shifted larvae (experiments as in Figure 6). The number of days larvae are kept at the non-permissive (Act5C^{OFF}) 29°C before switching to permissive 18°C are denoted. How these values correlate to FB cell size and development into flies is also noted.

F) FB cell sizes for control, *Act5C*^{RNAi}, and *ApoLpp*^{RNAi} larvae.

G) Proposed working model for role of Act5C in the fat body (FB).

Supplemental Figures:

Figure Supplement 1:

A) Confocal section images of tissue periphery (top) or mid-plane (bottom) of L3 non-wandering larval fat bodies (FBs) stained with Cell Mask™ Actin Tracking Stain (F-actin stain). Line-scans indicate actin signal across red dotted line in mid-plane. The *Dcg-Gal4* alone and *Dcg-Gal4>Act5C*^{RNAi} images are also in Figure 1C. Scale bar 10µm.

B) Z-section slices of confocal imaging of larval FB expressing plasma membrane marker mCD8-GFP (green), Act5C-RFP (red, Fire-LUT), and stained for LDs (MDH stain, blue).

Figure Supplement 2:

A) Confocal section images of tissue periphery (top) or mid-plane (bottom) of L3 non-wandering larval fat bodies (FBs) stained with LD stain MDH. Red boxes denote single FB cells. The *Dcg-Gal4* alone and *Dcg-Gal4>Act5C*^{RNAi} images are also in Figure 2. Scale bar 10µm.

B) Brightfield micrographs of isolated FBs from *Dcg-Gal4* control or *Dcg-Gal4>Act5C*^{RNAi} L3 non-wandering larvae. These are thick-section samples utilized for thin-section TEM microscopy. The peripheral LDs (pLDs) and medial LDs (mLDs) are marked. Scale bar 25µm.

Figure Supplement 3:

A) Fluorescent micrographs of L3 larval FBs stained for LDs (MDH). Peripheral (top) and mid-plane (bottom) zoomed-in views are shown for *Dcg-Gal4* control tissue as well as several RNAi lines depleted in the FB via *Dcg-Gal4*. Scale bar 10µm.

Figure Supplement 5:

A) Relative triglyceride (TG) of L3 non-wandering larval mid-guts from *Dcg-Gal4* control, *Dcg-Gal4>Act5C*^{RNAi}, and *Dcg-Gal4>ApoLpp*^{RNAi}).

B) Whole-larval diacylglycerol (DAG) from *Dcg-Gal4* control or *Dcg-Gal4>ApoLpp*^{RNAi} larvae.

C) Immuno-fluorescence confocal micrograph of human Huh7 hepatocytes immuno-stained for ApoB (green), the ER network (anti: calnexin, red), and co-stained for LDs (MDH, blue). Red arrows indicate ApoB. Scale bar is 4μm.

D) Negative stain thin section transmission electron microscopy (TEM) of L3 non-wandering larvae. Samples are either from control, *Act5C*^{RNAi}, or *ApoLpp*^{RNAi} larvae. Red arrows indicate Lpp-like particles. Blue stars indicate Lpp-like particles in pockets of extracellular space at the micro-ridges of the FB tissue periphery. Scale bar is 2μm.

E) Relative whole-larval (L3, non-wandering) triglyceride (TG) levels for several *Dcg-Gal4*>RNAi lines compared to *Dcg-Gal4* control larvae.

F) Confocal images of L3 non-wandering larvae from control or *Act5C*^{RNAi} samples, and expressing Golgi-marker *UAS-dGRASP65-GFP*. Scale bar is 10μm.

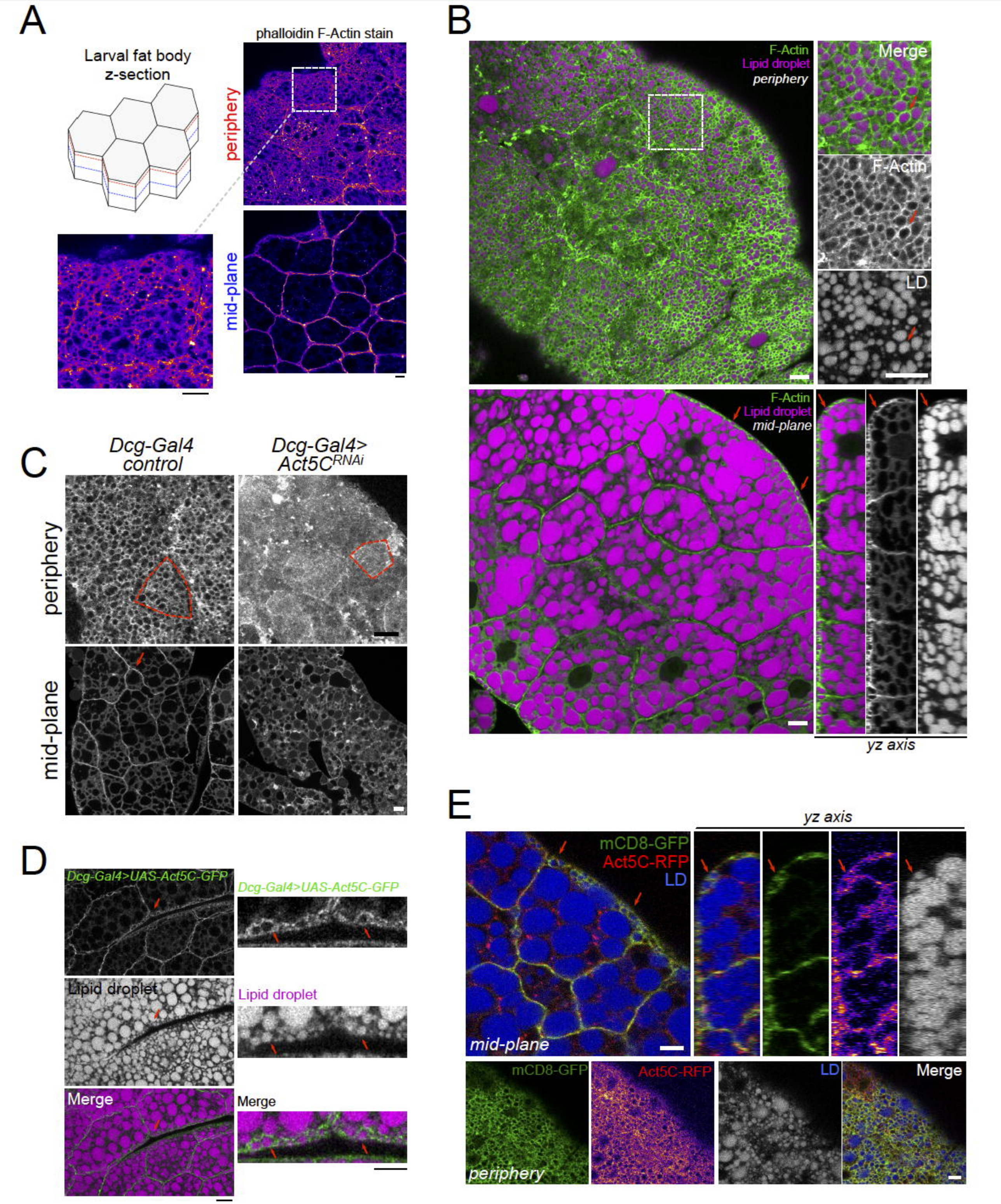
A
Larval fat body
z-section
phalloidin F-Actin stain
periphery
mid-plane
B
F-Actin
Lipid droplet
periphery
Merge
F-Actin
LD
F-Actin
Lipid droplet
mid-plane
yz axis
C
Dcg-Gal4
control
Dcg-Gal4>
Act5C^RNAi
periphery
mid-plane
D
Dcg-Gal4>UAS-Act5C-GFP
Dcg-Gal4>UAS-Act5C-GFP
Lipid droplet
Lipid droplet
Merge
Merge
E
yz axis
mCD8-GFP
Act5C-RFP
LD
mid-plane
mCD8-GFP
Act5C-RFP
LD
Merge
periphery

Figure 1

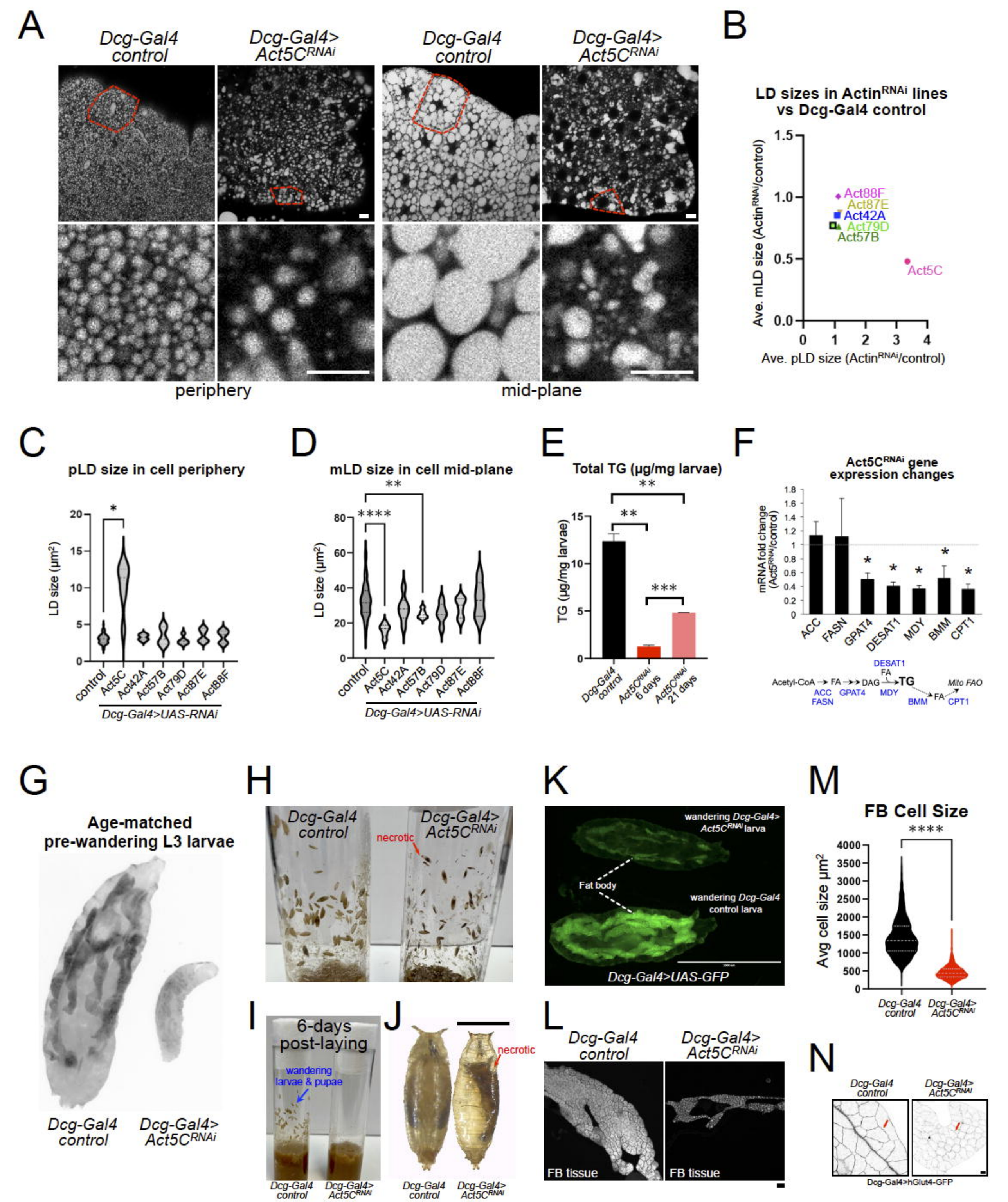
A
Dcg-Gal4 control
Dcg-Gal4> Act5C RNAi
Dcg-Gal4 control
Dcg-Gal4> Act5C RNAi
periphery
mid-plane
B
LD sizes in Actin RNAi lines vs Dcg-Gal4 control
Ave. mLD size (Actin RNAi/control)
Ave. pLD size (Actin RNAi/control)
Act88F
Act87E
Act42A
Act79D
Act57B
Act5C
C
pLD size in cell periphery
LD size (µm²)
control
Act5C
Act42A
Act57B
Act79D
Act87E
Act88F
Dcg-Gal4>UAS-RNAi
D
mLD size in cell mid-plane
LD size (µm²)
Dcg-Gal4>UAS-RNAi
E
Total TG (µg/mg larvae)
TG (µg/mg larvae)
Dcg-Gal4 control
Act5C RNAi 6 days
Act5C RNAi 21 days
F
Act5C RNAi gene expression changes
mRNA fold change (Act5 RNAi/control)
ACC
FASN
GPAT4
DESAT1
MDY
BMM
CPT1
Acetyl-CoA → FA → DAG → TG
FA
Mito FAO
G
Age-matched pre-wandering L3 larvae
Dcg-Gal4 control
Dcg-Gal4> Act5C RNAi
H
Dcg-Gal4 control
Dcg-Gal4> Act5C RNAi
necrotic
I
6-days post-laying
wandering larvae & pupae
Dcg-Gal4 control
Dcg-Gal4> Act5C RNAi
J
necrotic
Dcg-Gal4 control
Dcg-Gal4> Act5C RNAi
K
wandering Dcg-Gal4> Act5C RNAi larva
Fat body
wandering Dcg-Gal4 control larva
Dcg-Gal4>UAS-GFP
L
Dcg-Gal4 control
Dcg-Gal4> Act5C RNAi
FB tissue
FB tissue
M
FB Cell Size
Avg cell size µm²
Dcg-Gal4 control
Dcg-Gal4> Act5C RNAi
N
Dcg-Gal4 control
Dcg-Gal4> Act5C RNAi
Dcg-Gal4>hGlut4-GFP

Figure 2

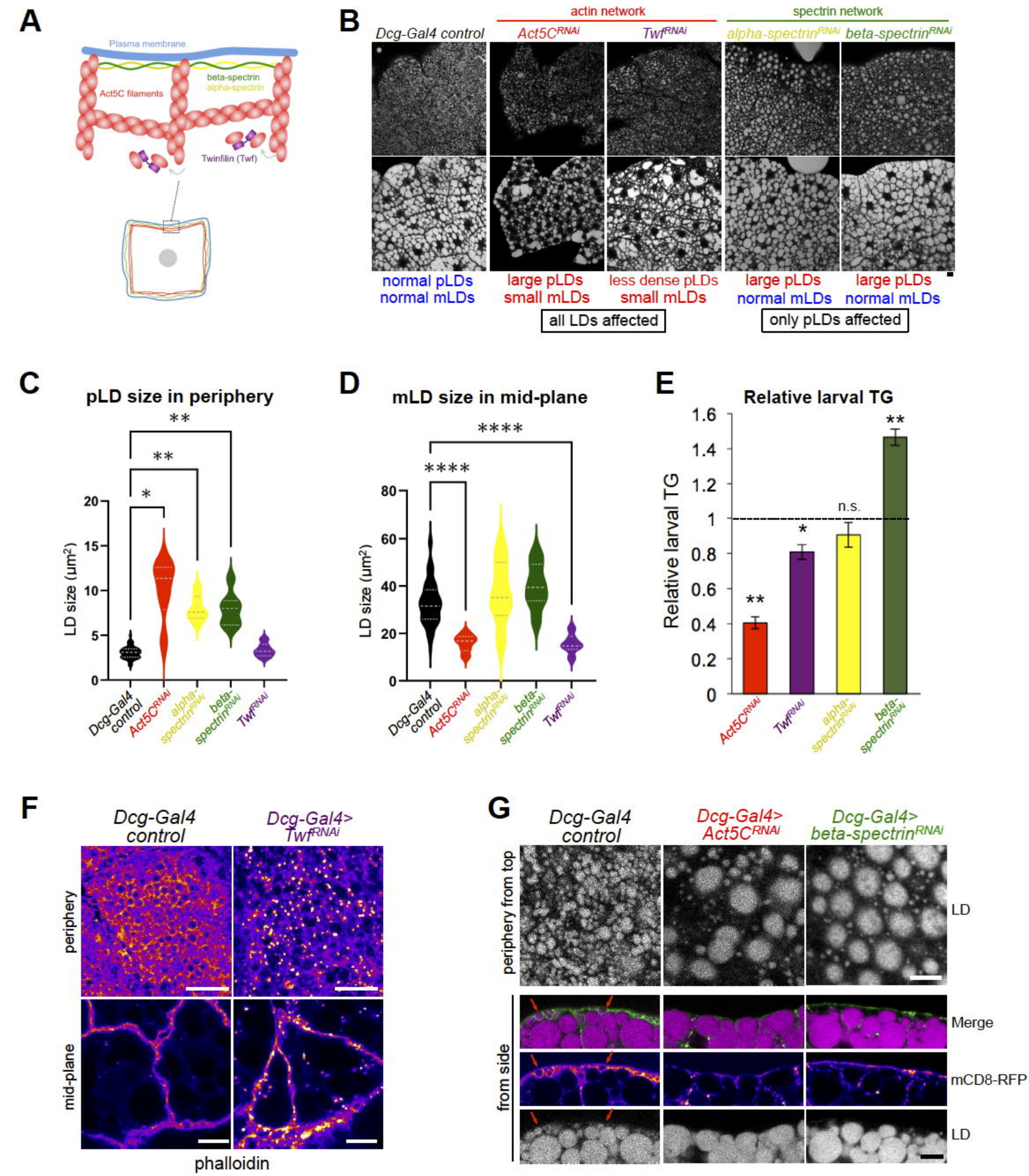
A
Plasma membrane
beta-spectrin
alpha-spectrin
Act5C filaments
Twinfilin (Twf)
B
actin network
spectrin network
Dcg-Gal4 control
Act5C RNAi
Twf RNAi
alpha-spectrin RNAi
beta-spectrin RNAi
normal pLDs
normal mLDs
large pLDs
small mLDs
less dense pLDs
small mLDs
large pLDs
normal mLDs
large pLDs
normal mLDs
all LDs affected
only pLDs affected
C
pLD size in periphery
LD size (µm²)
Dcg-Gal4 control
Act5C RNAi
alpha-spectrin RNAi
beta-spectrin RNAi
Twf RNAi
D
mLD size in mid-plane
LD size (µm²)
E
Relative larval TG
Relative larval TG
n.s.
F
Dcg-Gal4 control
Dcg-Gal4> Twf RNAi
periphery
mid-plane
phalloidin
G
Dcg-Gal4 control
Dcg-Gal4> Act5C RNAi
Dcg-Gal4> beta-spectrin RNAi
periphery from top
from side
LD
Merge
mCD8-RFP
LD

Figure 3

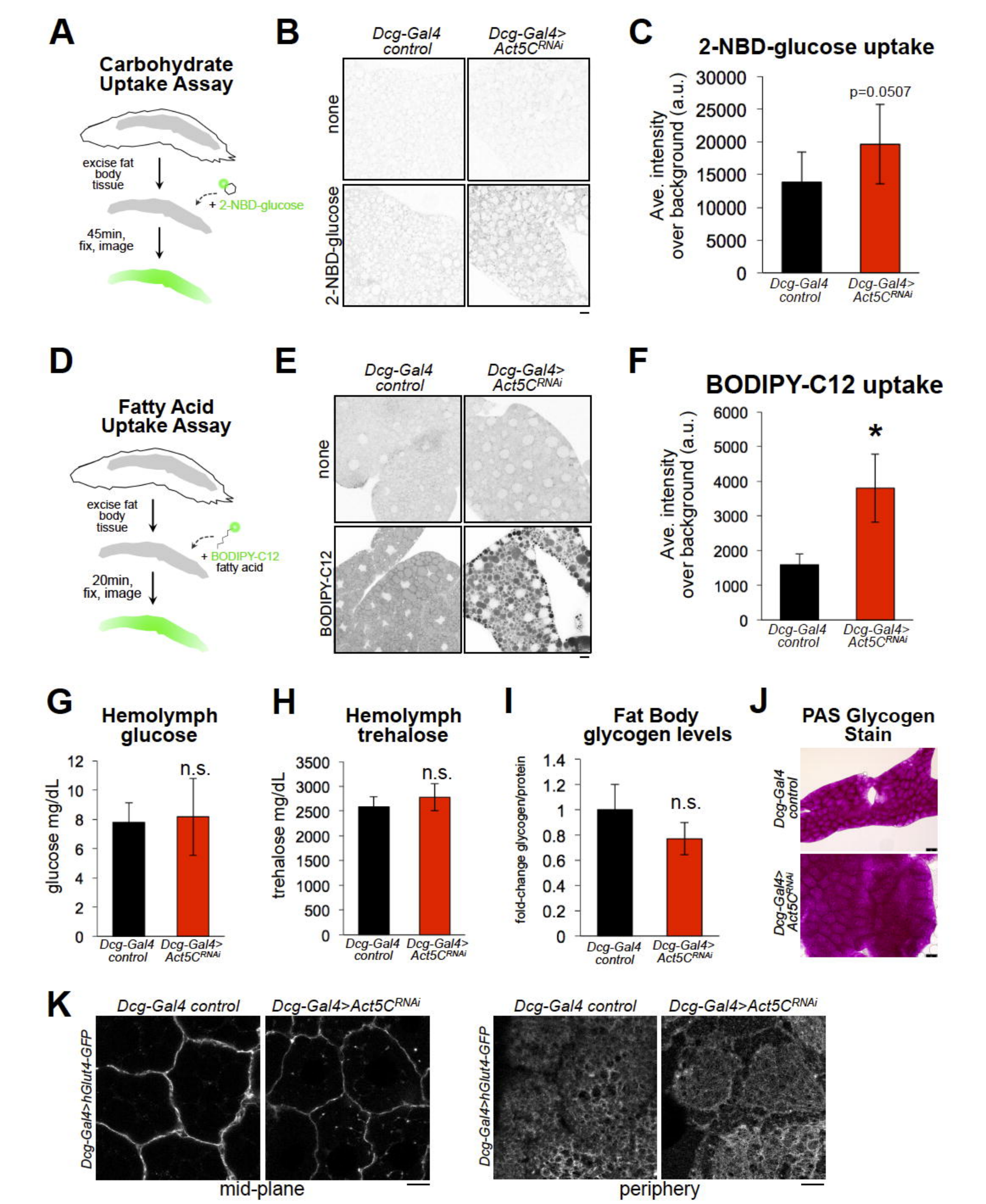
A
Carbohydrate Uptake Assay
excise fat body tissue
+ 2-NBD-glucose
45min, fix, image
B
Dcg-Gal4 control
Dcg-Gal4> Act5C^RNAi
none
2-NBD-glucose
C
2-NBD-glucose uptake
Ave. intensity over background (a.u.)
30000
25000
20000
15000
10000
5000
0
p=0.0507
Dcg-Gal4 control
Dcg-Gal4> Act5C^RNAi
D
Fatty Acid Uptake Assay
excise fat body tissue
+ BODIPY-C12 fatty acid
20min, fix, image
E
Dcg-Gal4 control
Dcg-Gal4> Act5C^RNAi
none
BODIPY-C12
F
BODIPY-C12 uptake
Ave. intensity over background (a.u.)
6000
5000
4000
3000
2000
1000
0
*
Dcg-Gal4 control
Dcg-Gal4> Act5C^RNAi
G
Hemolymph glucose
glucose mg/dL
12
10
8
6
4
2
0
n.s.
Dcg-Gal4 control
Dcg-Gal4> Act5C^RNAi
H
Hemolymph trehalose
trehalose mg/dL
3500
3000
2500
2000
1500
1000
500
0
n.s.
Dcg-Gal4 control
Dcg-Gal4> Act5C^RNAi
I
Fat Body glycogen levels
fold-change glycogen/protein
1.4
1.2
1
0.8
0.6
0.4
0.2
0
n.s.
Dcg-Gal4 control
Dcg-Gal4> Act5C^RNAi
J
PAS Glycogen Stain
Dcg-Gal4 control
Dcg-Gal4> Act5C^RNAi
K
Dcg-Gal4 control
Dcg-Gal4>Act5C^RNAi
Dcg-Gal4>hGlut4-GFP
mid-plane
Dcg-Gal4 control
Dcg-Gal4>Act5C^RNAi
Dcg-Gal4>hGlut4-GFP
periphery

Figure 4

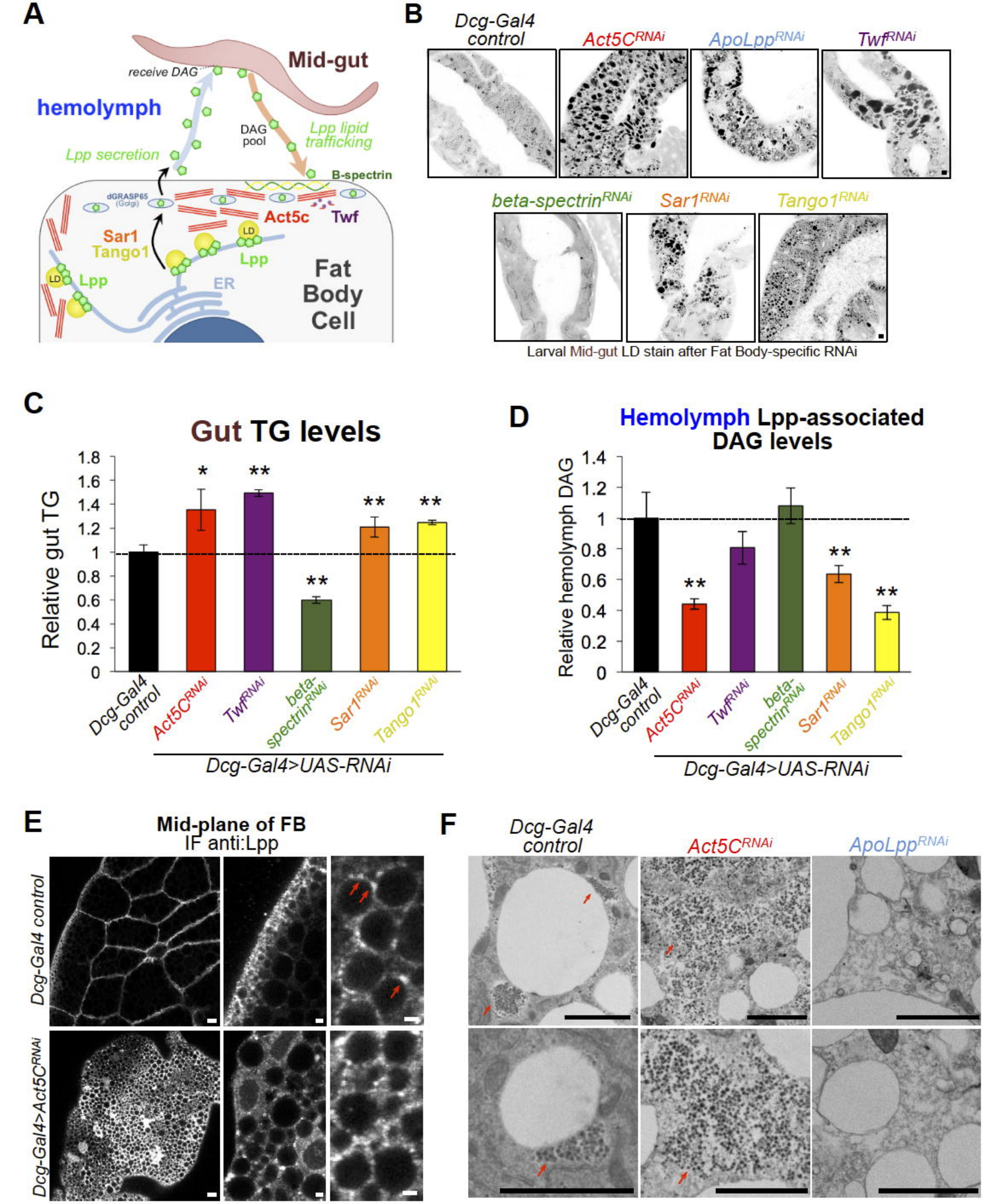
A
Mid-gut
receive DAG
hemolymph
DAG pool
Lpp lipid trafficking
Lpp secretion
B-spectrin
dGRASP65 (Golgi)
Act5c
Twf
Sar1
Tango1
LD
Lpp
ER
Fat Body Cell
B
Dcg-Gal4 control
Act5C RNAi
ApoLpp RNAi
Twf RNAi
beta-spectrin RNAi
Sar1 RNAi
Tango1 RNAi
Larval Mid-gut LD stain after Fat Body-specific RNAi
C
Gut TG levels
Relative gut TG
1.8
1.6
1.4
1.2
1
0.8
0.6
0.4
0.2
0
*
**
**
**
**
Dcg-Gal4 control
Act5C RNAi
Twf RNAi
beta-spectrin RNAi
Sar1 RNAi
Tango1 RNAi
Dcg-Gal4>UAS-RNAi
D
Hemolymph Lpp-associated DAG levels
Relative hemolymph DAG
1.4
1.2
1
0.8
0.6
0.4
0.2
0
**
**
**
Dcg-Gal4 control
Act5C RNAi
Twf RNAi
beta-spectrin RNAi
Sar1 RNAi
Tango1 RNAi
Dcg-Gal4>UAS-RNAi
E
Mid-plane of FB
IF anti:Lpp
Dcg-Gal4 control
Dcg-Gal4>Act5C RNAi
F
Dcg-Gal4 control
Act5C RNAi
ApoLpp RNAi

Figure 5

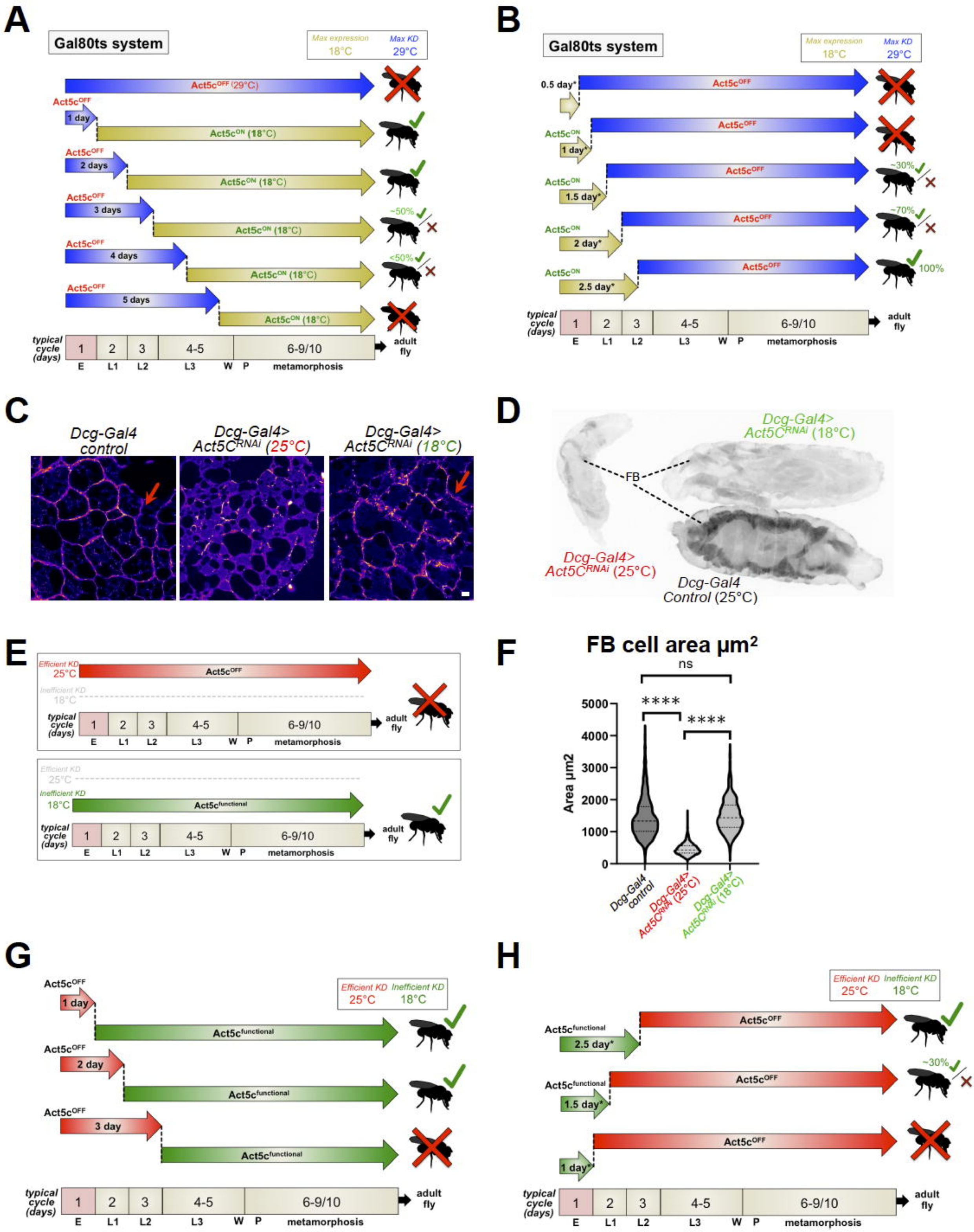
A
Gal80ts system
Max expression 18°C
Max KD 29°C
Act5c^OFF (29°C)
Act5c^OFF 1 day
Act5c^ON (18°C)
Act5c^OFF 2 days
Act5c^ON (18°C)
Act5c^OFF 3 days
~50%
Act5c^ON (18°C)
Act5c^OFF 4 days
<50%
Act5c^ON (18°C)
Act5c^OFF 5 days
Act5c^ON (18°C)
typical cycle (days)
1 2 3 4-5 6-9/10
E L1 L2 L3 W P metamorphosis
adult fly
B
Gal80ts system
Max expression 18°C
Max KD 29°C
0.5 day*
Act5c^OFF
Act5c^ON 1 day*
Act5c^OFF
Act5c^ON 1.5 day*
Act5c^OFF
~30%
Act5c^ON 2 day*
Act5c^OFF
~70%
Act5c^ON 2.5 day*
Act5c^OFF
100%
typical cycle (days)
1 2 3 4-5 6-9/10
E L1 L2 L3 W P metamorphosis
adult fly
C
Dcg-Gal4 control
Dcg-Gal4> Act5C^RNAi (25°C)
Dcg-Gal4> Act5C^RNAi (18°C)
D
Dcg-Gal4> Act5C^RNAi (18°C)
FB
Dcg-Gal4> Act5C^RNAi (25°C)
Dcg-Gal4 Control (25°C)
E
Efficient KD 25°C
Act5c^OFF
Inefficient KD 18°C
typical cycle (days)
1 2 3 4-5 6-9/10
E L1 L2 L3 W P metamorphosis
adult fly
Efficient KD 25°C
Inefficient KD 18°C
Act5c^functional
typical cycle (days)
1 2 3 4-5 6-9/10
E L1 L2 L3 W P metamorphosis
adult fly
F
FB cell area µm²
ns
****
****
Area µm2
5000
4000
3000
2000
1000
0
Dcg-Gal4 control
Dcg-Gal4> Act5C^RNAi (25°C)
Dcg-Gal4> Act5C^RNAi (18°C)
G
Act5c^OFF 1 day
Act5c^functional
Act5c^OFF 2 day
Act5c^functional
Act5c^OFF 3 day
Act5c^functional
Efficient KD 25°C
Inefficient KD 18°C
typical cycle (days)
1 2 3 4-5 6-9/10
E L1 L2 L3 W P metamorphosis
adult fly
H
Efficient KD 25°C
Inefficient KD 18°C
Act5c^functional 2.5 day*
Act5c^OFF
Act5c^functional 1.5 day*
Act5c^OFF
~30%
1 day*
Act5c^OFF
typical cycle (days)
1 2 3 4-5 6-9/10
E L1 L2 L3 W P metamorphosis
adult fly

Figure 6

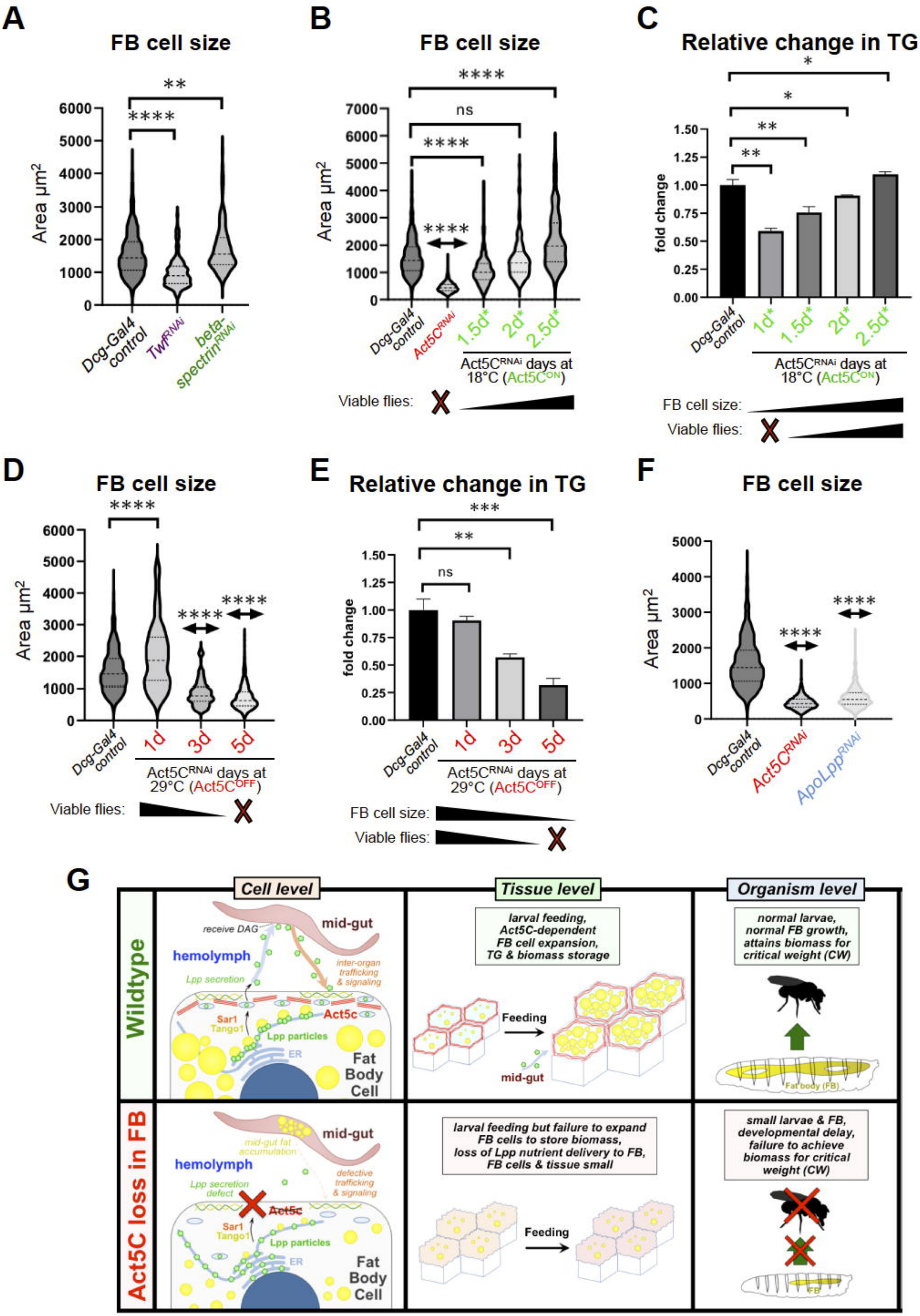
A
FB cell size
Area µm²
Dcg-Gal4 control
Twf RNAi
beta-spectrin RNAi
B
FB cell size
Dcg-Gal4 control
Act5C RNAi
1.5d*
2d*
2.5d*
Act5C RNAi days at 18°C (Act5C ON)
Viable flies:
C
Relative change in TG
fold change
FB cell size:
Viable flies:
D
FB cell size
1d
3d
5d
Act5C RNAi days at 29°C (Act5C OFF)
E
Relative change in TG
F
FB cell size
ApoLpp RNAi
G
Cell level
Tissue level
Organism level
Wildtype
Act5C loss in FB
mid-gut
hemolymph
receive DAG
Lpp secretion
inter-organ trafficking & signaling
Sar1
Tango1
Act5c
Lpp particles
ER
Fat Body Cell
larval feeding, Act5C-dependent FB cell expansion, TG & biomass storage
Feeding
normal larvae, normal FB growth, attains biomass for critical weight (CW)
Fat body (FB)
mid-gut fat accumulation
Lpp secretion defect
defective trafficking & signaling
larval feeding but failure to expand FB cells to store biomass, loss of Lpp nutrient delivery to FB, FB cells & tissue small
small larvae & FB, developmental delay, failure to achieve biomass for critical weight (CW)
FB

Figure 7

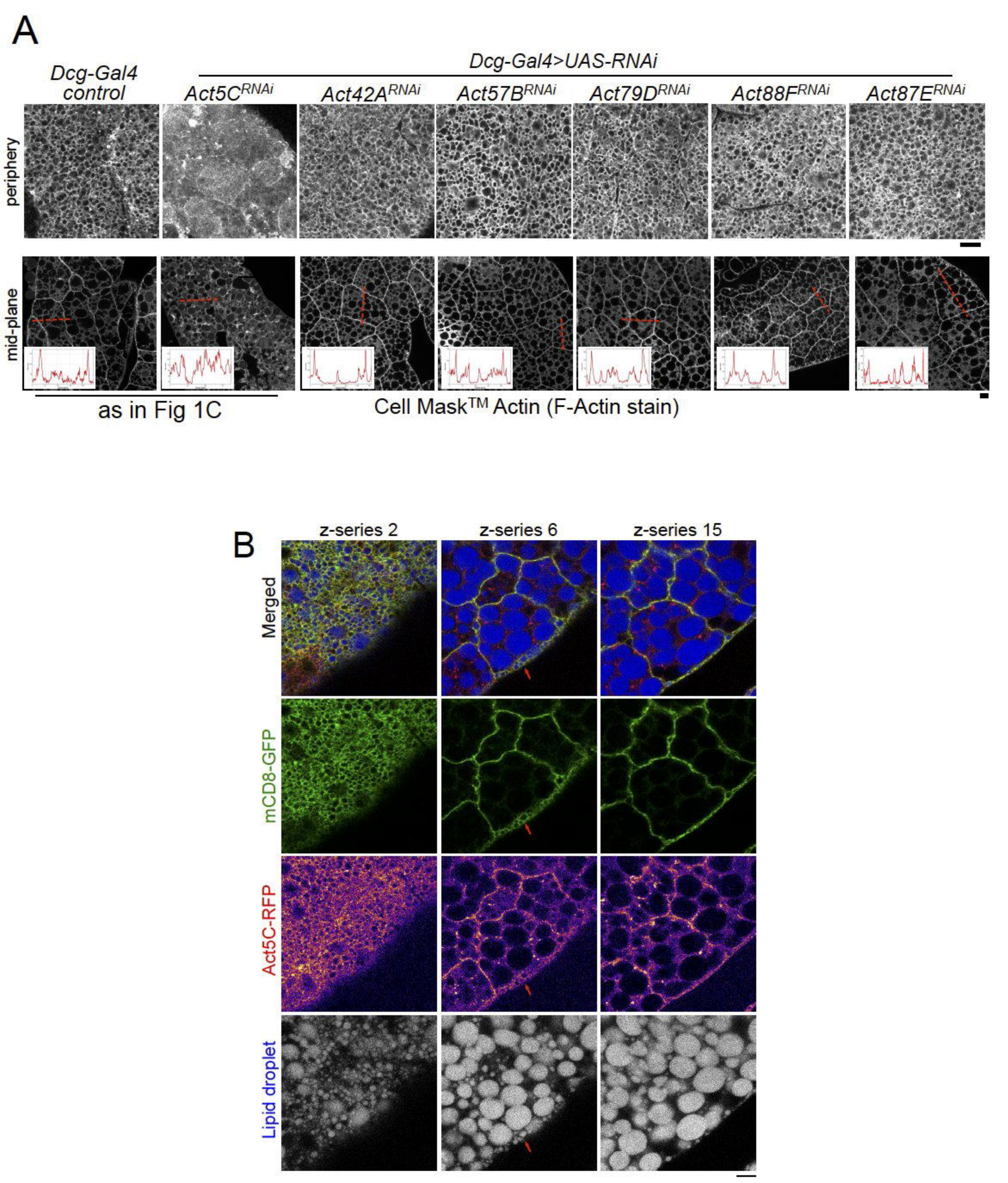

Figure Supplement 1

A

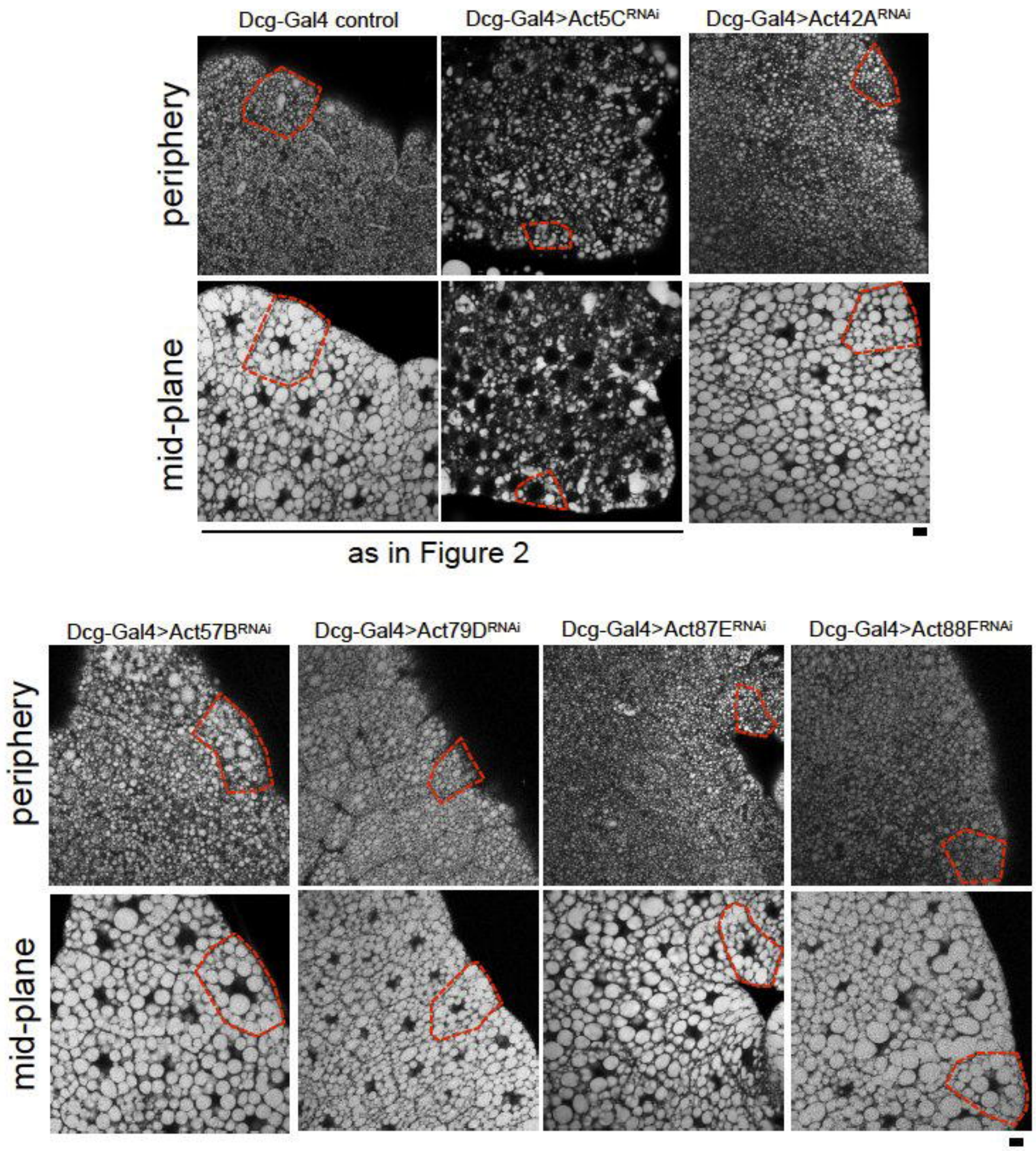

B

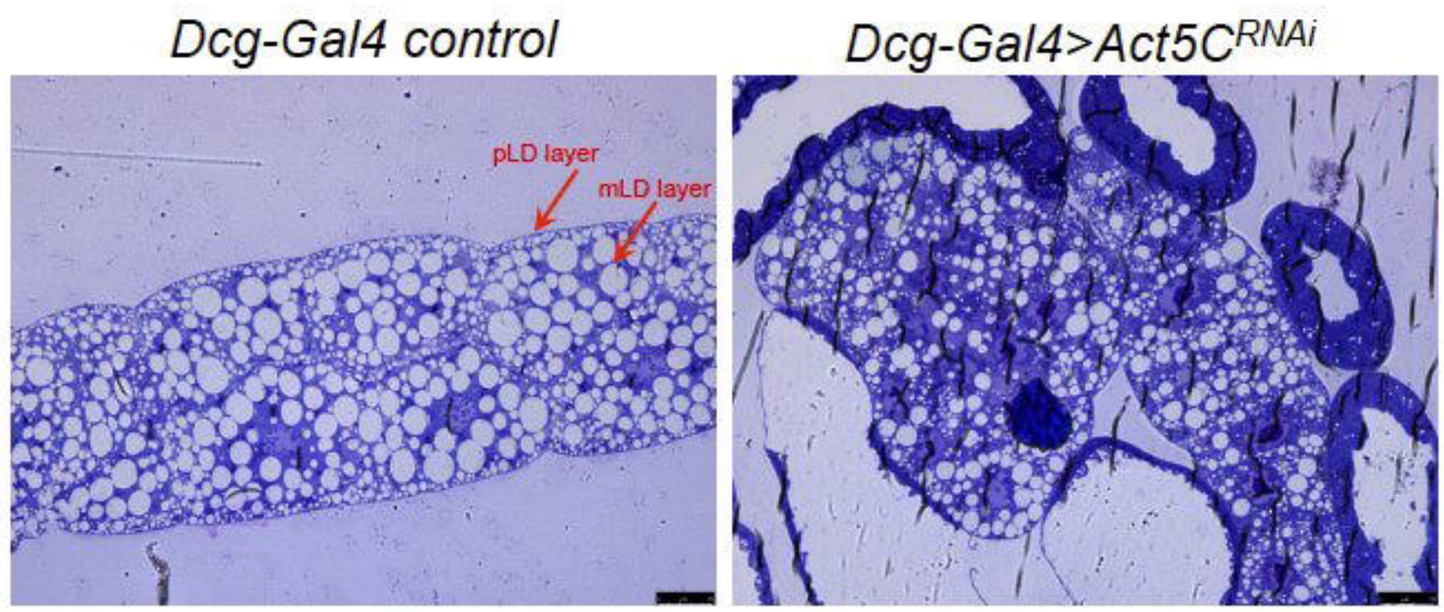

Figure Supplement 2

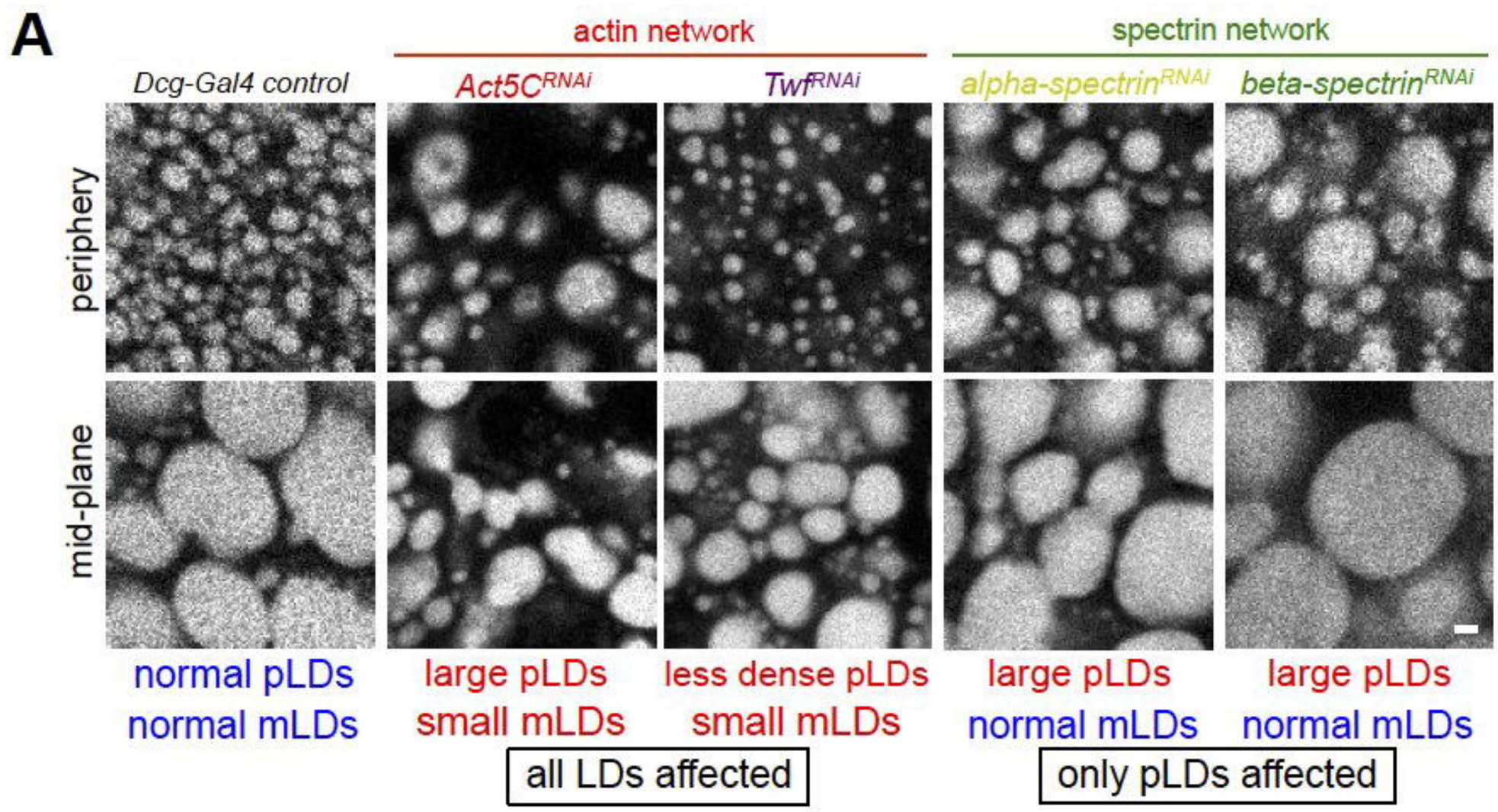
A
actin network
spectrin network
Dcg-Gal4 control
Act5C RNAi
Twf RNAi
alpha-spectrin RNAi
beta-spectrin RNAi
periphery
mid-plane
normal pLDs
normal mLDs
large pLDs
small mLDs
less dense pLDs
small mLDs
all LDs affected
large pLDs
normal mLDs
large pLDs
normal mLDs
only pLDs affected

Figure S3

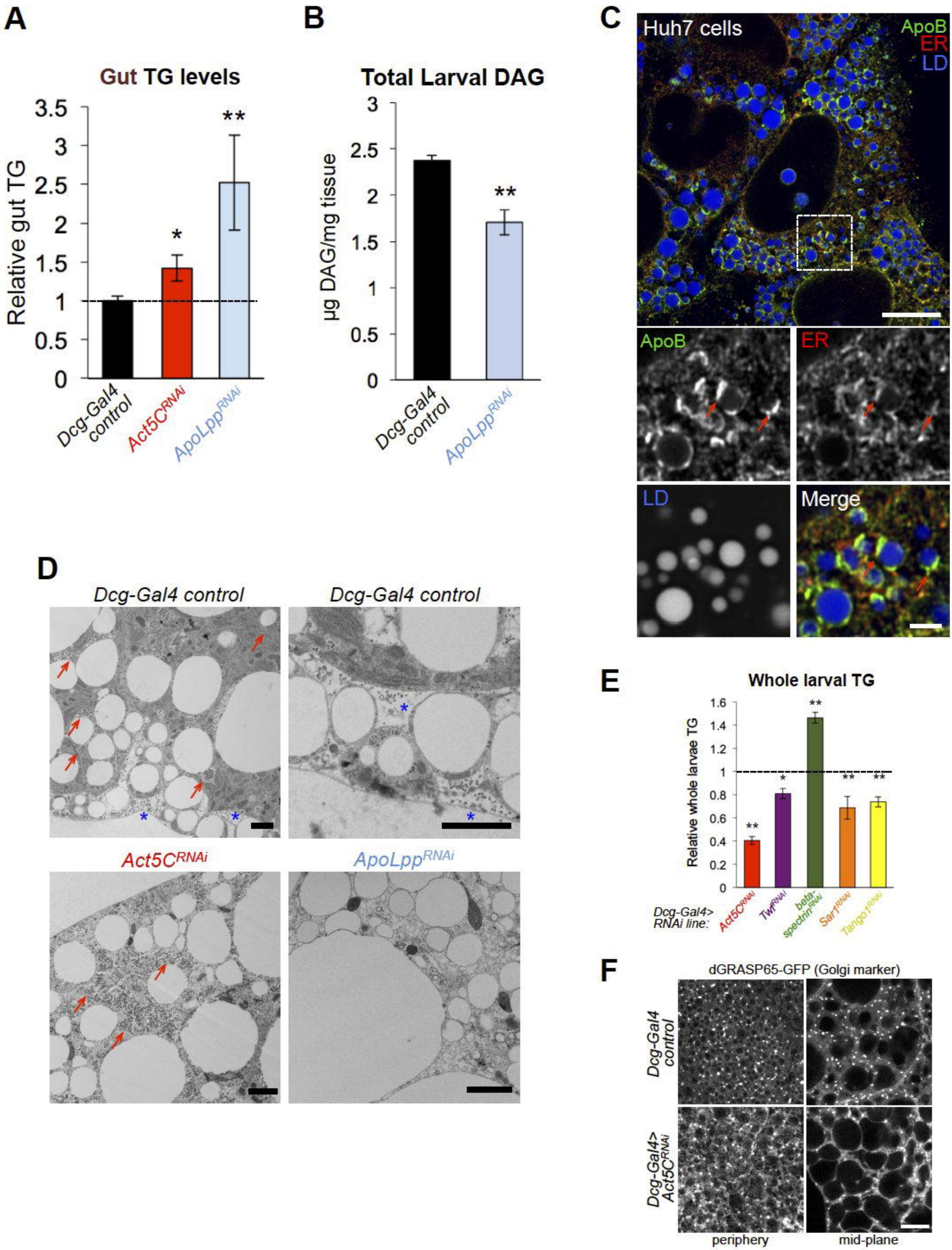

Figure Supplement 5